Towards simulations on the dynamics of colloidal coagulation

Beljon, R.

Award date:
2021

EINDHOVEN UNIVERSITY OF TECHNOLOGY

Department of Chemical Engineering and Chemistry
Laboratory of Physical Chemistry &
Chemical Process Intensification Research Group

Towards Simulations on the Dynamics of Colloidal Coagulation

MSc thesis

Roos Beljon, BSc

Committee:
prof. dr. ir. Remco Tuinier
dr. ir. Ivo Roghair
dr. ir. Mark Vis
dr. ir. Frank Peters

Eindhoven, June 2020

Abstract

Colloidal dispersions are extremely sensitive to coagulation and fouling. This limits industry to increase the productivity of polymerization processes. Numerical simulations can provide more insight into the parameters that affect coagulation. This study describes the development of a time-driven model that can simulate colloidal behavior in non-equilibrium circumstances, in which an ever-ongoing trade-off between efficiency and accuracy is present. The non-equilibrium circumstances are induced by phenomena at length scales different from the colloidal size, such as polydispersity and shear flow. The basic understanding of the open-source program LAMMPS and its application to the physical system has a significant role in this work.

High accuracy of the physical properties of colloidal particles, in particular their interactions, is an essential requirement for the model. The hard sphere model is well developed and therefore used as a reference system to tune the particle behavior. The Langevin thermostat is used to impose the solvent dynamics. For diluted systems, the Langevin damping coefficient has to be sufficiently high to make sure the colloidal particles resemble Brownian behavior.

Polydispersity can induce depletion forces in a system. It is not practical to model depletion forces by explicitly modeling the depletant particles. The depletion potential is also not one of the implemented potentials in LAMMPS. Therefore, two methods are discussed that fit multiple Yukawa potentials to the depletion potential. A 5-tails Yukawa potential has the best efficiency-resemblance ratio. The standard deviation only decreases 5% by the addition of another Yukawa tail.

Coagulation is bound to occur more often in shear flow. However, implicit solvents do not take shear forces into account. Several methods are discussed to obtain a simple shear flow of the colloidal particles with implicit solvent dynamics. The effect of shear on colloidal particles has been modeled by the addition of an external force. Additional friction on the particles is to be imposed by this force. The colloid-wall interactions do not have a significant contribution to the velocity profile in the case of diluted systems.

Contents

Chapter 1

Introduction

Polymers are remarkably involved in human life. Not only natural polymers are responsible for life itself, but also synthetic polymers are essential in our every day lives. The synthetic polymers are involved in all kinds of applications such as medication, nutrition, transportation, clothing, and construction (Namazi, 2017). The majority of the synthetic polymer production is performed with suspension or emulsion polymerization. These techniques involve the dispersion of monomers, polymers, or intermediate products in small particles (Kroupa et al., 2014), called colloids. In this study, the focus lies on emulsion polymerization. Yearly, over 13 million tonnes of emulsion polymers are produced and the market still has an annual growth of 6.9% (Distler et al., 2017, Cheng et al., 2018). Dispersions bring the benefits of both rate control and heat control (Mayer, 1995). However, dispersions also bring along some difficulties. Colloidal systems are thermodynamically unstable, which makes them very sensitive for coagulation and fouling. The particles are kinetically stabilized by surfactants to prevent cluster formation. In quiescent conditions, this is sufficient to prevent clustering of the particles (Kroupa et al., 2014, Cheng et al., 2018). However, in industry, where mixing and plug flow are essential for high production rates, the quiescent conditions are easily disturbed. Non-desired coagulation formation affects the product quality, causes loss of product, increases reactor downtime, and reduces the efficiency of heat exchange (Cheng et al., 2018).

The polymer industry desires more insight into coagulation phenomena and the corresponding mitigation strategies to increase production efficiency. Currently, most polymerization processes take place in batch or semi-batch reactors (González et al., 2007). With a better understanding of the fouling processes, a step can be made towards continuous polymerization reactions in tubular reactors (Pauer, 2017). This insight can be gained by performing numerical simulations. In numerical simulations, parameters influencing coagulation phenomena can easily be tuned, allowing for relatively fast and inexpensive research. However, it requires an accurate and efficient numerical model that can predict the behavior of colloidal particles.

The development of a numerical model for colloidal systems is particularly challenging. The system contains a wide range of particle sizes and interactions. More specific for coagulation, the clustering occurs by both diffusive and convective forces. These take place at different length scales. Modeling many length scales and physical properties in the same system is computationally demanding. Nevertheless, several numerical models are developed in recent years (Zinchenko and Davis, 1995, Lattuada and Morbidelli, 2011, Elgebrandt et al., 2005). Simplifications have to be imposed on the colloidal system to make the model computationally feasible. Therefore, most of these models focus on just one aspect of the coagulation process.

The purpose of this work is to develop an efficient 3D numerical simulation model that can accurately describe coagulation phenomena. Much attention is paid to the colloidal dynamics. This could result in a model that can cope with both the diffusive and convective coagulation effects. To ensure optimized algorithms, LAMMPS is used as a framework for the model. LAMMPS is an open-source

molecular dynamics code. The program is known for its combination of versatility and excellent parallel performance. Furthermore, the code can easily be extended, which is done daily by the active user community (Plimpton, 2014). If creators approve the extensions created by the users of LAMMPS, the code is integrated and updated for all users. Hence, the program keeps evolving rapidly.

The thesis is structured as follows. The theoretical background explains the emulsion polymerization system and discusses the most likely causes of coagulation. Based on this theory, the first simplifications for the model are introduced. The understanding of the basic principles of LAMMPS together with the extension and validation of a new pair style takes up a large part of this study. The basic structure and commands of the LAMMPS input script are explained in the technical background. The solvent plays a crucial role in the dynamics of colloids. The theory of the colloid behavior in the diluted regime is well developed, especially for particles with hard sphere interactions (Fortini et al., 2005, Dhont, 1996). In Chapter 4 the solvent dynamics are tuned to make sure the fundamental physical properties of a colloidal system resemble in the simulations. This is first done for hard sphere colloidal particles and later extended to particles with a Yukawa interaction. In Chapters 5 and 6, the model is extended to investigate possible causes of coagulation, respectively polydispersity and shear forces. The focus in these Chapters remains on the development of an efficient modeling method. The work is finalized with a discussion, conclusion, and elaborate outlook.

Chapter 2

Theoretical background

In the development of numerical models there is always a trade-off between the number of details that can be modeled and the computational time. The challenge is to make sure the simulations stay an accurate representation of reality while making simplifications in the modeled system. To do well-founded simplifications, it is of importance to have a thorough understanding of the system. As is elaborated in the introduction, the reference system of this study is the process of emulsion polymerization. In this section, a short description of the process is given. Furthermore, the possible causes of coagulation and their corresponding significant length scales are discussed. Lastly, the theory of colloidal diffusion is explained, since it is of importance that the simulations can accurately describe the diffusive behavior of the colloidal particles.

2.1 Emulsion polymerization

Emulsion polymerization is a free radical polymerization proceeding in a heterogeneous system. The main ingredients besides the continuous aqueous phase comprise monomer, initiator, and surfactant (Iqbal and Ahmad, 2018, Yamak, 2013). The surfactants work as a stabilizing agent in the system. In the initial configuration, a small fraction of monomer is solubilized by the micelles, an even smaller fraction is dissolved by the aqueous phase, and the vast majority is located in monomer droplets. The droplets act as a reservoir of monomers during the polymerization (Distler, 2001, Yamak, 2013). The polymerization is initiated by the addition of an initiator. This happens at a temperature around 80 °C. The polymerization happens mainly in the monomer swollen micelles. As the polymerization proceeds, the polymer-swollen micelles grow and the monomer droplets shrink. After the monomer droplets have entirely disappeared, the final phase of the reaction commences. In this phase, polymerization continues within the polymer-swollen micelles until the monomer conversion is almost 100% (Distler et al., 2017, Yamak, 2013). Finally, the result is a dispersion of polymer particles stabilized by surfactants, also called latex. The polymer particles obtain very high molecular weights on the order of 1,000,000 monomer units or higher (Lewarchik, 2016).

2.2 Coagulation mechanisms

Two mechanisms for coagulation can be distinguished; perikinetic coagulation and orthokinetic coagulation. These can also co-occur. Brownian motion of particles facilitates perikinetic clustering. The Brownian motion brings particles into intimate proximity of one another. Orthokinetic clustering results from the movement of the fluid. Velocity gradients in the flow field can increase the force of collisions as well as the collision frequency (Cheng et al., 2018). When the colloidal particles approach each other multiple forces start to play a role. The van der Waals forces are attractive forces arising from electric dipoles in the molecules. Furthermore, there are repulsive electrostatic forces (also called double layer forces), which depend on the electric charge at the surface of the particles

(Cheng et al., 2018, Lekkerkerker and Tuinier, 2011). A second repulsive force is a steric force. These forces arise from hydrophilic tails bound to the surface of the particle (Cheng et al., 2018). These chains occupy a certain space. Therefore, the entropy of the chains decreases in the close proximity of other chains (Pinter et al., 2012). Solvation forces can also contribute to the repulsive character of a particle (Cheng et al., 2018). The solvated particles have interactions with the surrounding solvent molecules. Hydrophilic chains that form hydrogen bridges with the water molecules are an example. These interactions have to be (partially) broken before the particles can coagulate. The last force, which is particularly interesting in this system, is the depletion force. Non-adsorbing particles/-molecules have an effective depletion layer near the particle surface due to the loss of configurational entropy in that region (Lekkerkerker and Tuinier, 2011). When the particles approach each other and the depletion layers start to overlap, more volume is available for the non-adsorbing particles. Thus the free energy of the system minimizes when the colloidal particles are close together (Lekkerkerker and Tuinier, 2011). In the emulsion polymerization system, there is a large amount of non-adsorbing particles and molecules that can induce depletion forces.

In the specific case of depletion polymerization, the opinions on the coagulating particle type are not uniform. Ouzineb et al. (2004) claim that the problem is linked to the presence of monomer droplets in the dispersion. Asua (2016) shares this opinion. He says that the large monomer droplets cream and thereby form a layer at the surface of the reactor, which upon polymerization leads to clogging. However, the majority of the articles speak of coagulation of polymer particles in their research (Pokorný et al., 2016, Yamak, 2013, Cheng et al., 2018).

2.3 Length scales

It is crucial to choose the right length scale to work with to increase the efficiency of the computations. The right length scale is selected based on the sizes of the investigated particles and the dominating forces. The length scale determines the simplifications that can be done while keeping an accurate representation of reality.

Emulsion polymerization is especially a complex system due to the numerous time and length scales that play a role in the system. On every length scale, complex dynamic processes take place; several simultaneous and competitive colloidal (aggregation, coalescence), chemical (radical generation, polymerization, termination, chain transfer), and physical (diffusion, nucleation, swelling) events occur (Hernandez and Tauer, 2008). An emulsion polymerization system contains monomers and surfactants in the size range of 1-50 Å, micelles in the size range 2-10 nm, polymer particles in the size range 10-1000 nm, and monomer droplets in the size range 1-100 μm (El-hoshoudy, 2018).

To ease the computational demand, the focus of this research is shifted towards the colloidal particles in the system, which include the monomer droplets and polymer particles. The corresponding length scale is called the mesoscopic scale. In this scale, colloidal suspensions are frequently modeled as atomic systems whose inter-particle interactions can be tuned (Laurati et al., 2009, Poon, 2016). The colloidal particle, which consists of many molecules, is course-grained into one big particle, see Figure 2.1. The monomer droplets and polymer particles are approximated as perfect spheres in the model. The spherical geometry is the favored configuration for these colloidal particles to minimize the surface tension (El-hoshoudy, 2018). The impact of external forces on a colloidal particle increase strongly with its size. For the large monomer droplets, these forces, like gravity, can play a role. However, for the more substantial part of the colloidal regime, external forces can be neglected (Dhont, 1996, Cheng et al., 2018). In this part of the regime, the dominating forces are the inter-particle forces. The change of velocity will, therefore, only be determined by the interactions with other colloidal particles and the forces induced by the solvent.

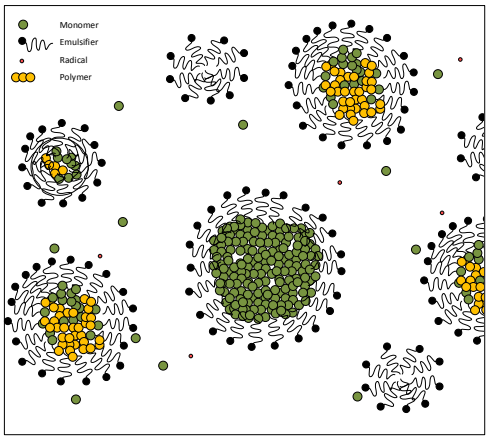

(a) A schematic overview of the emulsion polymerization system.

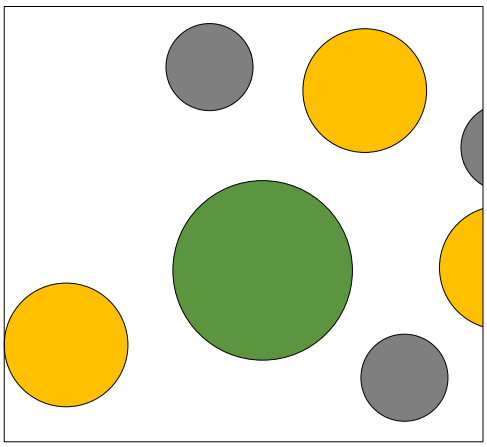

(b) The emulsion polymerization system as it is modeled with simplifications.

Figure 2.1: The course-graining simplification performed on the colloidal dispersion.

2.4 Colloidal diffusion

Diffusion describes how a particle displaces itself over time and is thus strongly dependent on the type of motion the particle exhibits. Colloids typically show thermal motion, called Brownian motion. The motion is caused by many random collisions with the fast-moving solvent molecules (Dhont, 1996).

There are two types of diffusion processes to be distinguished: collective and self-diffusion. Collective diffusion relates to the motion of many Brownian particles simultaneously, caused by density gradients (Russel et al., 1991). Self-diffusion takes place without concentration gradients. The movement occurs because of the random motion of a Brownian particle excited by thermal fluctuations, under the influence of interactions with surrounding Brownian particles (Dhont, 1996). The latter type of diffusion is particularly interesting because it can indicate which type of particle interactions are in play.

The mean square displacement (MSD) is a simple measurable quantity that characterizes the motion of a single Brownian particle, defined as,

$$\mathrm{MSD}(t) = \langle |p(t) - p(t=0)|^2 \rangle, \tag{2.1}$$

where $p(t)$ is the position coordinate of the particle at time t (Dhont, 1996). The mean square displacement for a Brownian particle consists of two regimes, indicated in Figure 2.2. For minimal times, the particle did not yet change its velocity due to collisions with solvent molecules; this is called the ballistic regime (Dhont, 1996). In this regime, the mean squared displacement is equal to,

$$MSD(t) = v^2(t=0)t^2. \tag{2.2}$$

After the ballistic regime, the particle suffers many random collisions with the solvent molecules. This leads to many random changes of its velocity and thus reducing its displacement with time as compared to ballistic motion (Dhont, 1996), resulting in a linear relationship between the mean squared displacement and time,

$$MSD(t) = 6D_s t. \tag{2.3}$$

In this equation, D_s is the self-diffusion coefficient. For a single hard sphere through a pure solvent the self-diffusion coefficient can be calculated via the Stokes-Einstein equation. In this case, D_s is

equal to D_0.

$$D_0 = \frac{k_B T}{6\pi\mu a}. \tag{2.4}$$

The denominator represents the amount of friction factor, i.e. the drag experienced by the particle. The friction of the particle depends on the viscosity of the fluid, μ, and the radius of the particle, a, only.

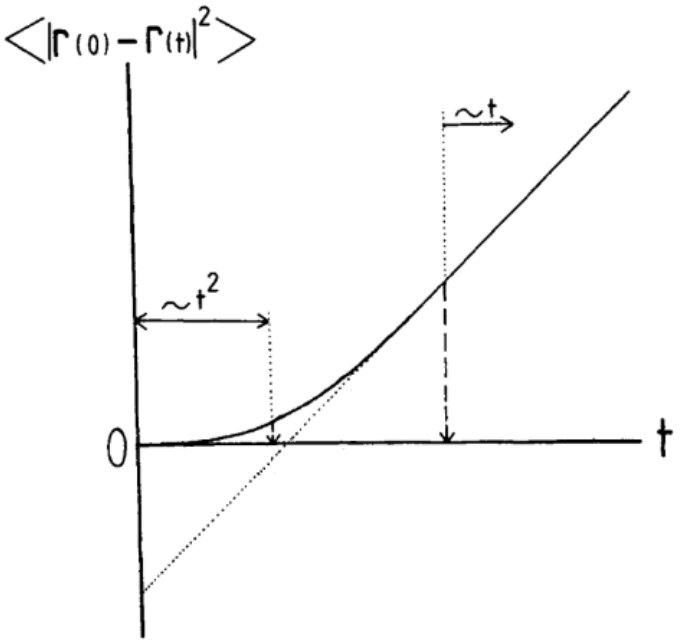

Figure 2.2: The mean square displacement of a Brownian particle as function of time (Dhont, 1996).

In the presence of other Brownian particles, the self-diffusion coefficient is no longer equal to D_0. Interactions of a particle with its surroundings affect the time dependence of the mean squared displacement; the diffusion coefficient changes (Dhont, 1996). Colloidal systems provide a wide variety of interparticle interactions, including the hard sphere system. The hard sphere interaction is extensively used as a reference potential. A rigorous insight into the hard sphere behavior is imperative for understanding all other interactions where excluded volume is of importance (Dullens, 2005).

The self-diffusion regime can now be split into two regimes: short-time self-diffusion and long-time self-diffusion. In the short-time self-diffusion regime, the diffusion of the Brownian particles is altered because of flow effects induced by other particles. Batchelor (1976) derived for this regime an expression for the short-time self-diffusion coefficient as a function of the interaction potential. For hard sphere interactions, the expression for the self-diffusion coefficient is

$$D_s^S = D_0[1 - 1.832\phi]. \tag{2.5}$$

This equation predicts the hard sphere diffusion coefficient well for the low volume fraction of the colloidal particles, $\phi < 0.05$ (Dhont, 1996). At higher volume fractions, three-body interactions start to play a role, which makes the expression for the diffusion coefficient much more complicated (Cichocki et al., 1999). In the long-time self-diffusion regime, the Brownian particles start to collide with each other. This regime is valid when MSD $\gg a^2$. The diffusion coefficient can now be expressed by

$$D_s^L = D_0[1 - 2.0972\phi]. \tag{2.6}$$

For simulations where only the particle size is changed, the diffusion coefficient is inversely proportional to the size of the particle. This enables us to validate the model by comparing the ratio between the radii and diffusion coefficients.

$$D_s \sim \frac{1}{a} \tag{2.7}$$

Particle interactions beyond the hard sphere limit the Brownian particles in their movement. For both repulsive and attractive interactions, the mean square displacement decreases, and with that also the self-diffusion coefficient. Baxter (Baxter, 1968) developed in 1968 the sticky hard sphere model. In this model he introduced the stickiness parameter, τ, which can be linked to short-ranged attractions. Subsequently, Cichoki (Cichocki and Felderhof, 1990) derived an expression for the self-diffusion coefficient of hard spheres with a short-ranged attraction. The expressions for short-time and long-time self diffusion are respectively:

$$D_s^S = D_0[1-(1.832+0.295/\tau)\phi], \tag{2.8}$$

$$D_s^L = D_0[1-(2.0972+0.562/\tau)\phi]. \tag{2.9}$$

The variable τ can be derived from the second virial coefficient, B_2. Also B_2 is a measure of the interaction between two particles. The value of this property can be calculated using Equation 2.10, which is depending on the interaction potential. τ is directly related to B_2 by Equation 2.11.

$$B_2 = 2\pi \int_0^\infty r^2(1-\exp[-U(r)/k_B T])\mathrm{d}r. \tag{2.10}$$

$$\frac{B_2}{v_c} = 4-\frac{1}{\tau}. \tag{2.11}$$

The range of interaction is defined as a certain ratio of the particle diameter. As long as the relative range of interaction is kept constant, τ does not vary with the size of the particles. This means that when diffusion coefficients of hard sphere particles with a short-range attraction are compared, they should still follow the inversely proportional relationship to the size of the particle.

Chapter 3

Technical background

The simulations in this study are performed using LAMMPS (Plimpton et al., 2020), which stands for Large-scale Atomic/Molecular Massively Parallel Simulator. It is a classical molecular dynamics code that models ensembles of particles in a liquid, solid, or gaseous phase (Sandia Corporation, 2020). The code of LAMMPS is written in C++. The total program consists of over a hundred different files, all connected. It is possible to use the program as a black box. However, the code is open-source and hence it is also possible to quickly look into the code and extend the code (Sandia Corporation, 2020). In this study, the LAMMPS version of august 2019 is used. Furthermore, the simulations are performed on a computer with an Intel Core CPU (i9-7940x) with 28 cores at 3.10GHz with 32 GB random access memory (RAM). The simulations are performed with Lennard-Jones (LJ) units. This means that all quantities are unitless. There are three fundamental quantities for distance, energy, and mass, respectively σ, ϵ, and m. These quantities are set to 1. All other quantities are multiples of those three. All quantities expressed in this work are expressed by the LJ units, indicated by the *. Moreover the relation between LJ- and real units can be found in Appendix B.

An input script has to be created with the structure and commands recognized by LAMMPS. In this chapter, the basic structure of a LAMMPS input file is described towards the simulation of colloidal systems. Moreover, there is some extra attention paid to modeling concepts as cutoff distances and time integration. Furthermore, the hard sphere model for time-driven simulations is discussed in detail.

3.1 Input script structure

The LAMMPS program can be run from a terminal. In the terminal, the path to the input script can be given using the '-in' flag. By default, the working directory is also the location where the output is stored. The structure of the input script is of great importance, since the program does not read the entire input script and then performs the simulation, but rather executes by reading the commands one line at the time (Sandia Corporation, 2020). The input script typically consists of 4 parts: initialization, system definition, simulation settings, and run section. Below, these parts are explained more extensively, including typical commands that have been used in the simulations. Putting all these pieces of code together does not form the whole input script, but cover the basics. A complete input script of a hard sphere colloidal system with implicit solvent dynamics is given in Appendix A.

3.1.1 Initialization

Every input script starts with defining the units, the particle type, and the dimension of the simulation (Plimpton, 2014). In this research, Lennard-Jones units are used. The atom style indicates the particle type. The choice of style affects what quantities are stored by each particle. These quantities are communicated between the processors, and thereby used to compute forces (Sandia Corporation,

2020). The atom style used for this project is `sphere`. The corresponding attributes coupled to this atom style are diameter, mass, and angular velocity. These quantities are sufficient to describe the colloidal particle behavior. It is possible to use more complicated atom styles. However, this is not computationally efficient. In this work, always a three-dimensional model is used.

```
units           lj
atom_style      sphere
dimension       3
```

3.1.2 System definition

The simulation environment has to be created. The box shape, box size, number of particle types, and type of boundaries have to be defined (Plimpton, 2014). The simulation box in the model is cubic, and by exception rectangular. The diameters of the colloidal particles vary from 14 to 20 σ. To have a fair comparison between the different simulations, the volume fraction is kept constant. The box dimensions for the different particle sizes are listed in Appendix C. Figure 3.1 shows the mean square displacement for systems containing 100 and 1000 colloidal particles. Systems containing 100 particles have limited statistics, which shows itself in the fluctuations of the mean square displacement. The system with 1000 particles starts to look like the ideal mean square displacement curve of Figure 2.2. Because of the better statistics, systems of 1000 particles will be the default in this work. Only for the explicit solvent simulations a smaller number of particles is taken, this is further elaborated in Chapter 4. In the same command that creates the simulation box, the number of particle types has to be defined. For example, in a simulation where colloidal particles and solvent particles are modeled, there are two particle types. The boundaries of the simulation box can be set periodic(p), non-periodic and fixed(f), non-periodic and shrink-wrapped(s), and non-periodic and shrink-wrapped with a minimum value(m) (Sandia Corporation, 2020). Shrink-wrapping means that the boundaries adjust themselves to the positions of the particles, no matter how far they move. The defined boundary style is always applied to both faces of a dimension. For the diffusion simulations a box with full periodic boundaries is used. For simulations with shear, non-periodic fixed boundaries are applied in the y-dimension.

```
boundary        p p p
region          box block ${xmin} ${xmax} ${ymin} ${ymax} ${zmin} ${zmax}
create_box      2 box
```

Also part of the system definition is setting the initial particle positions and velocities. The particles can be placed in the system using LAMMPS commands or by loading an external file, with positions and velocities defined. In the developed model, both methods are combined. The colloidal particles are inserted via an external file, the solvent particles are placed with LAMMPS commands, and the velocity for both colloids and solvent particles is set using LAMMPS. When the LAMMPS commands are used, the `lattice` command plays an important role. In this command, the type of packing can be chosen (e.g. fcc, bcc, hpc) and the density of the particles is set. In the case of Lennard-Jones units the density is the reduced mass density, ρ^*. With the `create\_atoms` command particles are created on the lattice points in the simulation box. The placement of the `lattice` command in the input script has to be done with caution. After the `lattice` command is used, the default for the distance units is the lattice spacing in the x,y,z direction implied by the lattice. The external input file that contains the particle positions has to follow strict guidelines for LAMMPS to be able to read the file. It can occur that the colloid and solvent particles overlap in their initial positions. The `delete\_atom` command allows deleting solvent particles that are overlapping with the colloidal particles. If the program crashes in a simulation with the error 'lost atoms', the initial positions of two particles were most likely overlapping. If the overlap between particles becomes too big, the energy of the particles rises tremendously and extremely high forces are computed. This high force causes the particles to disappear from the system. The initial velocity is set by the `velocity` command. The velocities are

generated based on a given temperature, as described in

$$\sum_i \frac{1}{2} m_i \langle v_i^2 \rangle = \frac{3}{2} N k_B T. \tag{3.1}$$

The default temperature in this work is $1.0T^*$. The `velocity` command is one of the commands that makes use of a pseudo-random number generator (PRNG) that is initialized by a seed value. The random seed is used to create a pseudo-random velocity distribution over the indicated particles. Every time the same set of numbers is used, the same distribution is generated. This makes it easy to reproduce simulations.

```
read_data       c_inp.000.D14 add append
lattice         sc 0.76
create_atoms    2 box
delete_atoms    overlap 8 solvent colloid
velocity        all create 1.0 3344588
```

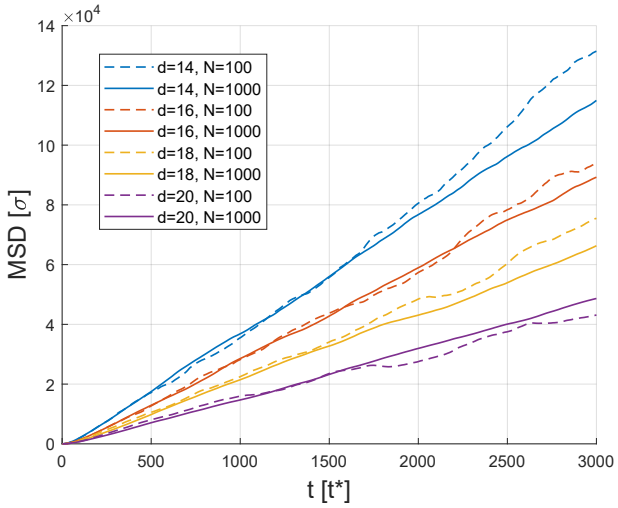

Figure 3.1: The mean square displacement for systems containing of 100 and 1000 colloidal particles.

3.1.3 Simulation settings

Once the particles and the system topology is defined, the force field and time-integration can be set. This part of the input script is the heart of the simulations. Two types of forces can be distinguished; external and multi-body forces. External forces act from outside the system on a single particle and are therefore independent of the position of other particles in the system (Shen et al., 2018). External forces can be implemented in the model by the `fix addforce` command. The command specifies what the magnitude of the force is, on which particles the force works, and which timesteps the force has to be executed. The external force plays a crucial role in Chapter 6 about shear. The multi-body forces do depend on the positions of other particles. These forces can be derived from the potential energy, U, which is a function of the distance between two particles, r.

$$F_i = -\nabla_i U(r_1, ..., r_N) \tag{3.2}$$

Multi-body forces are implemented with the `pair_style` command. This command allows for implementation of various well known potentials, as the Lennard-Jones, Coulomb and Yukawa potential (Sandia Corporation, 2020). The `pair_style` command is always followed by the `pair_coeff` command. In this latter command, the coefficients are set which are required for the specific pair style.

The number of required coefficients differs per pair style. However, `pair_coeff` is always first followed by the particle types on which the potential is applied. In the example code below, the pair style `colloid` is used. The coefficients defined in the `pair_coeff` command are respectively type 1, type 2, energy prefactor, size of the solvent particle, diameter type 1, diameter type 2, and cut-off. The program allows for the application of multiple pair styles in one simulation. With the `hybrid` style different pairs of particle types can have different interactions. With the `hybrid/overlay` style multiple pair styles can be assigned to the same pair of particle types. In this case, the potentials are accumulated.

The time integration is set with a `fix` command. This command can be used to define the ensemble that is applicable on the system. LAMMPS supports two numerical time-integration methods; Velocity-Verlet and r-Respa, of which velocity-Verlet is the default setting. These integration methods work very efficient and accurate, and above all, they are seamlessly integrated into the LAMMPS package. The high accuracy of the velocity-Verlet method is only retained as long as the force at time t only depends on the positions of the particles at time t, and not on the velocities at time t. For dissipative systems (where the force does depend on the velocity), the accuracy is generally lower, i.e. smaller time steps are needed to achieve a sufficient level of accuracy (Frenkel and Smit, 1996). The r-Respa method is based on the velocity-Verlet method, however the force is decomposed into short and long range forces. In the velocity-Verlet method the full force must be recomputed every time step. In the Respa method the short range force is computed after each time step and the long range force is computed every n time steps (Tuckerman et al., 1992). This makes it a multi-time scale integrator, which allows for different hierarchies of system properties in the system. In the next sections of this chapter, important aspects of the simulation settings obtain further elaboration, which concerns the calculation of forces, the used pair styles, and ensembles.

```
pair_style colloid

pair_coeff 1 1  39.5 1.0 14.0 14.0 35.0
pair_coeff 1 2  75.4 1.0 14.0 0.0 11.0
pair_coeff 2 2  144 1.0 0.0 0.0 2.5

fix         1 all nve
```

3.1.4 Run section

In this finalizing part of the input script, the desired output can be defined. LAMMPS offers four kinds of output: Thermodynamic output, dump files, user-specified quantities, and restart files. For this study, both the thermodynamic output and the dump files are extensively used. Dump files can store per-atom values and therefore are used to store the particle positions and velocities. This data is required for visualization tools (Ovito is used in this research). Thermodynamic data consists of system values. This data consists of energies, pressures, and also the mean square displacement. In this section also the `timestep` and `run` command are given. The timestep is of huge importance in the fidelity of the simulations. However, the smaller the timestep, the longer the computation time. In section 3.5, an analysis is done to determine the acceptable step size. The script closes with the `run` command in which the number of simulation steps is defined.

3.2 Calculating the inter-particle forces

As stated above, the multi-body forces are depending on the distance between particles. Calculation of the potential energies and the corresponding forces, therefore, requires the distance between a particle and all other particles in the system. For large systems with many particles, the calculation of the forces becomes very computationally expensive (Frenkel and Smit, 1996). The efficiency of the models is increased tremendously by the introduction of the neighbourlist. Neigbourlists are

based on the fact that particles have a certain interaction range beyond which the interactions are zero or so small that they may be neglected (Leach, 2001). This range is called the cut-off distance, R_{cut}. The neigbourlist contains only the particles that are close neigbours of each particle. The range that determines which particles are added to the neigbourlist is the cut off distance plus a certain shell thickness. This shell thickness is necessary to include already neigbours that may enter the cut-off radius. This way, the list does not have to be recreated every timestep (Leach, 2001). Figure 3.2 shows a schematic overview. The cutoff distance is set as a parameter in the `pair\_style` command. This cut-off distance should not be too large; otherwise particles that fall not within the interaction range are still added to the neigbourlist. But, more importantly, the cut-off distance should not be too small. The potential beyond the cut-off distance is set to zero. This means that if the original potential had not reached the zero value yet, the wrong cut-off causes a jump in energy. The energy jump can cause errors in the computation of the energy and forces. Below, in subsection 3.2.1, the trade-off between the computation time and the energy computation is elaborated further for the Lennard-Jones potential. Sometimes it is necessary to have a sizeable cut-off range, as is the case in long-range interactions. It is then important to allow the neigborlist to contain more particles than its default maximum. This can be done with the `neigh_modify` command.

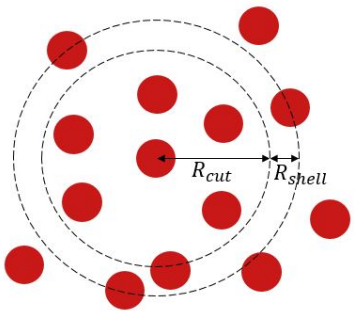

Figure 3.2: A schematic overview of the particles that lie within the range of the neigbourlist.

3.2.1 Lennard Jones cut-off

A general Lennard-Jones potential is shown in Figure 3.3. At considerable inter-particle distances the potential approaches the zero; there is no longer any interaction between the particles. However, when setting a cut-off, the transition between the energy before and after the cut-off is not always smooth. Even at very high cut-off distances, there is a jump in energy (ΔU), although this difference is minimal. The magnitude of the energy jump affects both the fluctuations and the average energy in the system. As the cut-off distance increases, the average energy starts to converge to constant energy of 0.962ϵ and the standard deviation approaches zero. In Figure 3.4, a line is fitted through the data points that represent the average energy and the standard deviation as a function of the cut-off distance. The corresponding expressions for the fitted lines are

$$f_{\text{avgE}}(x) = 330.3\,x^{-2.573} + 0.962, \tag{3.3}$$

$$f_{\text{std}}(x) = 1.282 \cdot 10^{5}\,x^{-4.953}. \tag{3.4}$$

The magnitudes of the exponents in the equations indicate that converging to the average energy is the limiting factor in determining the cutoff distance. With the converged energy value and the data points, a rate of convergence can be computed, shown in Table 3.1. The rate of convergence starts to decrease for cutoff distances larger than 100 σ. This, together with Table 3.2, helps to conclude that 150 is a reasonable cut-off, with minimal deviation of the converged value, minimal fluctuations, and minimal computation time.

Cutoff interval	Rate of convergence
25-50	2.562
50-100	2.821
100-200	2.127
200-400	0.773

Table 3.1: The rate of convergence towards final system energy. The rate is calculated between the cutoffs indicated in the cutoff interval.

Deviation of convergence	Minimal cutoff
1%	142
0.1%	347
0.01%	849

(a) Deviation of the convergence value.

Standard deviation	Minimal cutoff
0.0001	74
0.00001	118
0.000001	188

(b) Standard deviation

Table 3.2: The minimal required cut-off depending on restrictions set for the final average energy and fluctuations.

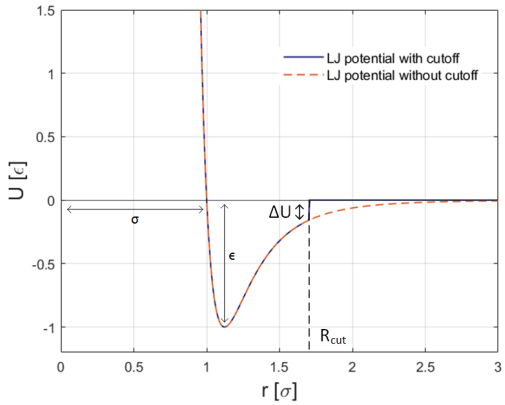

Figure 3.3: The Lennard-Jones potential with and without cutoff. ΔU indicates the energy jump that arises of a too small cutoff. The indicated σ and ϵ are essential quantities in the Lennard-Jones units.

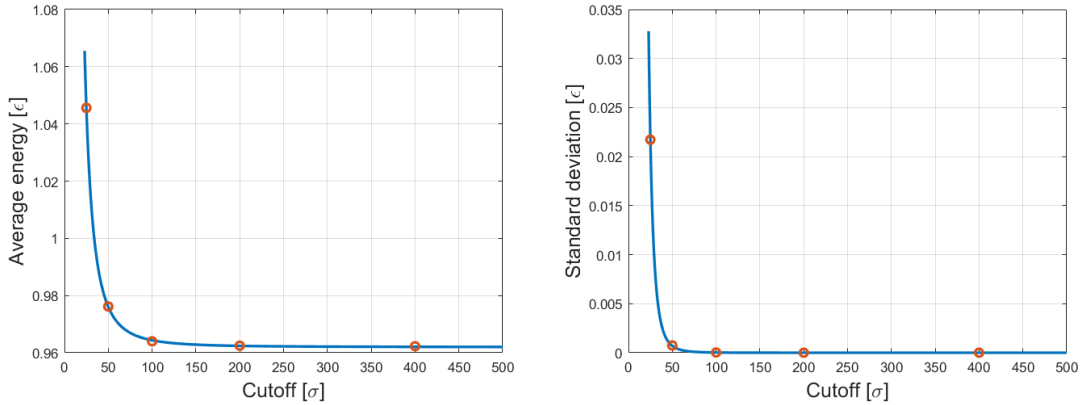

(a) Average system energy.

(b) Standard deviation.

Figure 3.4: The effect of the cut-off distance on the average system energy and energy fluctuations of a Lennard-Jones system. The blue line is fitted through the orange data points.

3.3 Pair styles

As explained, the pair styles in LAMMPS define which interaction potential exists between two particles. This work focuses on hard sphere interactions and later expands to Yukawa interactions.

3.3.1 Hard sphere interactions

The hard sphere (HS) model is a relatively simple and widely used approach (González García and Tuinier, 2016). Furthermore, the physical properties of a hard sphere colloidal dispersion are already thoroughly investigated (Fortini et al., 2005). This makes the hard sphere model particularly interesting to validate the model with. In a hard sphere interaction, two particles have infinite high repulsion towards each other when the surfaces touch. The ideal hard sphere potential can be described as,

$$U(h) = \begin{cases} \infty & h \leq 0 \\ 0 & h > 0 \end{cases}. \tag{3.5}$$

Potentials can be described as a function of both h and r. h indicates the distance between the two surfaces of the particles, where r indicates the distance between the centers of the particles. The perfect hard sphere potential is shown in Figure 3.5a.

Hard spheres can easily be modeled using event-driven simulations. The collisions in these simulations are instantaneous. However, time-driven simulations are favorable when interactions beyond the hard sphere regime are at play. Later in this study also this type of interaction will play a role. Therefore, the simulations are time-driven. However, this makes modeling the hard sphere interaction somewhat complicated. In the ideal hard sphere potential, the energies of the particles will go from zero to infinitely in one timestep; the resulting force would be infinite as well. Therefore, hard sphere interactions can only be approximated. The smaller the timestep of the simulation, the steeper the slope of the potential can be. According to Plimpton (2009), one of the authors of LAMMPS, the hard sphere potential can be approximated in two ways. With the right cut-off distance, $r_{\text{cut}} = 2^{\frac{1}{6}}\sigma$, and a shift of the potential with ϵ, the repulsive part of the Lennard-Jones potential can be used as the inter-particle potential.

$$U_{\text{LJ}} = 4\epsilon\left[\left(\frac{d}{r}\right)^{12} - \left(\frac{d}{r}\right)^{6}\right] + \epsilon. \tag{3.6}$$

Alternatively, the granular Hertz potential can be used with high stiffness. The stiffness can be created by setting the elastic constant for normal contact (k_n) high (around 100 p^*) and setting the viscoelastic damping constants(γ_n and γ_t) to zero.

$$U_{\text{gran}} = \sqrt{\delta}\sqrt{\frac{a_i a_j}{a_i + a_j}}\left[\left(k_n \delta n_{ij} - m_{\text{eff}}\gamma_n v_n\right) - \left(k_t \Delta s_t + m_{\text{eff}}\gamma_t v_t\right)\right] \tag{3.7}$$

The suggested pair potentials are evaluated for two particles of size 14 σ. The resulting pair potentials are shown in Figure 3.5b and 3.5c. What can be seen quickly is that the granular Hertz potential is a better approximation than the repulsive Lennard-Jones potential. The adjusted Lennard-Jones potential is a sufficient hard sphere approximation for small particle sizes. However, as the particle size increases, the potential becomes less steep. The granular Hertz potential shows a small decrease at the origin, which is the artifact of the well that describes the soft sphere collision. Jover et al. (2012) proposed to use the generalized cut-and-shifted Mie potential for the hard sphere approximation. The equation that describes this potential is shown in equation 3.8.

$$u_{\lambda_R,\lambda_A}(r) = \begin{cases} \frac{\lambda_R}{\lambda_R - \lambda_A}\left(\frac{\lambda_R}{\lambda_A}\right)^{\frac{\lambda_A}{\lambda_R - \lambda_A}} \epsilon\left[\left(\frac{d}{r}\right)^{\lambda_R} - \left(\frac{d}{r}\right)^{\lambda_A}\right] + \epsilon & r < d\left(\frac{\lambda_R}{\lambda_A}\right)^{\frac{1}{\lambda_R - \lambda_A}} \\ 0 & r \geq d\left(\frac{\lambda_R}{\lambda_A}\right)^{\frac{1}{\lambda_R - \lambda_A}} \end{cases} \tag{3.8}$$

In their research Jover et al. (2012) show that especially the choice for λ_R contributes to the hard sphere approximation. A compromise has to be made between the fidelity of the hard sphere representation

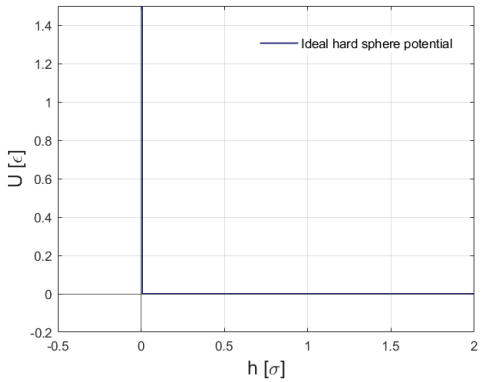

(a) HS potential.

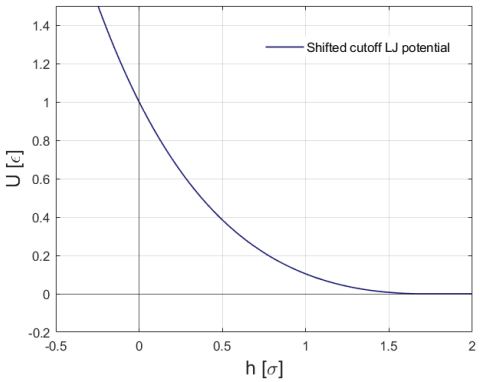

(b) Cut-and-shifted LJ potential.

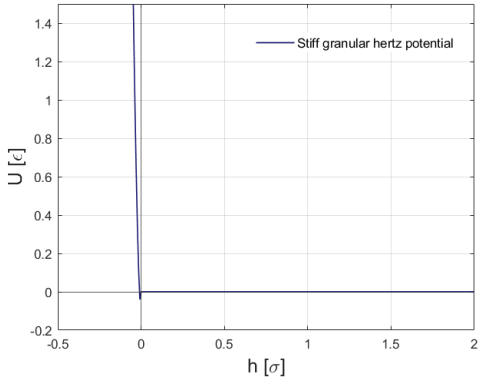

(c) Stiff granular Hertz potential.

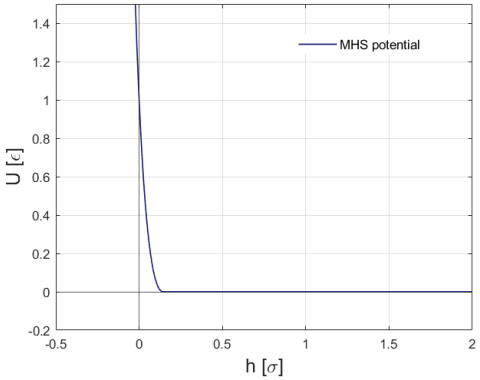

(d) MHS potential

Figure 3.5: The hard sphere potential approximations for particles of 14σ.

and the size of the time step in the simulation. The steeper the potential, the higher the fidelity. But also, the steeper the potential, the smaller the required timesteps. The values that are most often used for λ_r and λ_a are respectively 12 and 6. With these values, the cut-and-shifted Lennard-Jones potential is produced, which is the same potential as the first suggestion of Plimpton and depicted in Figure 3.5b.

In this work, the generalized cut-and-shifted Mie potential is further explored by changing the λ_r and λ_a values. The effect on the hard sphere behavior of a two-particle collision is investigated. The hard sphere behavior is measured in the maximal overlap at collision, furthermore, the computational limitation is based on the energy difference before and after the collision. The hard sphere collision is suppose to be fully elastic, which means that energy has to be conserved in the collision. The steeper the potential gets, the bigger the computational error becomes.

The Mie potential is implemented as one of the pair styles in LAMMPS. However, this potential is designed for monodisperse systems and is not automatically shifted. One of the advantages of the program LAMMPS, is the possibility to extend the code. To fully experience the features that LAMMPS has to offer, it has been decided to create a new pair style. This pair style is designed explicitly for colloidal hard sphere systems. The pair style is based on the generalized cut-and-shifted Mie potential. Since the LAMMPS code has a complicated structure, an already existing part of the code is taken as a reference. The reference pair style is the pair style `colloid` (Plimpton et al., 2020). This

pair style allows for a polydisperse system. Furthermore, the colloid-solvent and solvent-solvent interactions are defined in the same pair style. The Lennard-Jones potential defines the solvent-solvent interactions. The colloid-solvent interactions are derived by Everaers and Ejtehadi (2003). He derived the potential for finite-size particles by describing each colloidal particle as an integrated collection of Lennard-Jones particles.

$$U_{\text{cs}} = \frac{2a^3\sigma^3 A_{cs}}{9(a^2-r^2)^3}\left[1 - \frac{\left(5a^6+45a^4r^2+63a^2r^4+15r^6\right)\sigma^6}{15(a-r)^6(a+r)^6}\right], \tag{3.9}$$

where A_{cs} is the Hamaker constant, a the radius of the colloidal particle, and σ the size of the solvent particles. The new script has to be saved in the same directory as where the reference script is stored. With the new script included, the LAMMPS package has to be compiled and built again. This pair style is called the `MHS` (Mie Hard Sphere) pair style.

The exploration of the generalized Mie potential is performed with the `MHS` pair style. The timestep of the simulations is set to 0.001. The effect of λ_R and λ_A on the overlap and energy error of a two-particle collision8 is shown in Figure 3.6. Based on this figure the values for λ_R and λ_A are chosen to be respectively 100 and 95. With these parameters both the overlap and energy difference are kept minimal. Figure 3.5d shows the resulting potential. The steepness of this potential is slightly lower than for the granular Hertz potential. The main difference between the two is the starting point of the repulsion. For the `MHS` pair style, this already slightly starts before $h = 0$. Both the `granular/hertz`

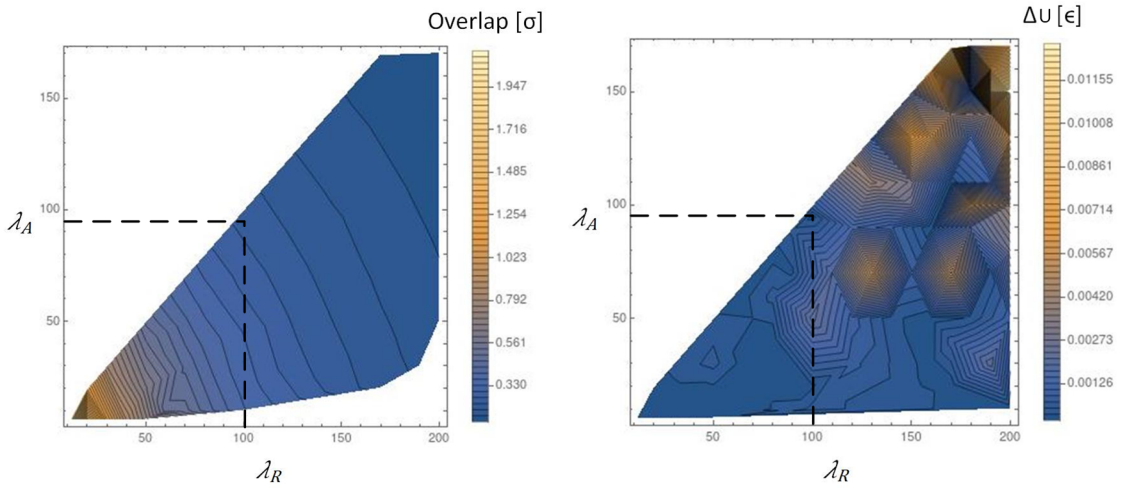

(a) The overlap between two particles in a collision.

(b) The energy difference, arising due to a numerical error.

Figure 3.6: The effect of λ_R and λ_A on the suitability for a hard sphere potential.

and `MHS` pair style are reasonable hard sphere approximations. To determine the best potential, a final energy analysis is performed. The energy analysis as performed previously in Figure 3.6b focuses on the energy of one collision. Meanwhile, the energy in this analysis is the total energy of a system with 100 particles simulated over a longer period of time. Again a system is desired that conserves energy. Looking at Figure 3.7, the `MHS` pair style shows a much more constant energy. In a closer look, it appears that the `MHS` pair style is not entirely constant. However, the standard deviation is merely of the order $10^{-6}\epsilon$. The standard deviation for the `granular/hertz` pair style is of the order $10^{-4}\epsilon$. The `MHS` pair style will further be used as the hard sphere approximation.

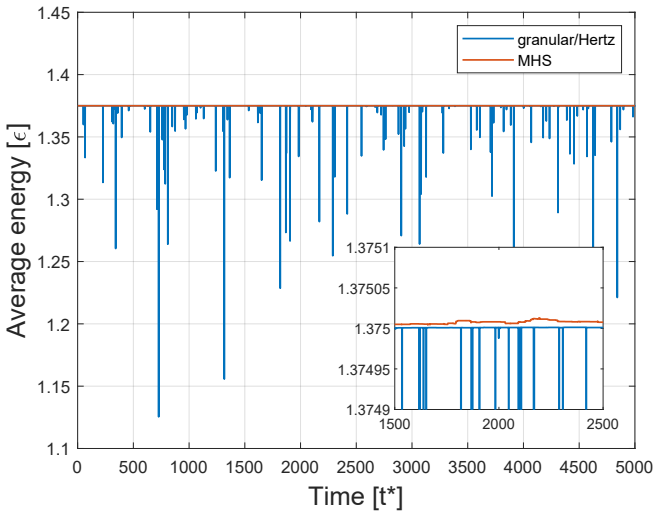

Figure 3.7: The total system energy during the simulation for `granular/hertz` particles and `MHS` particles.

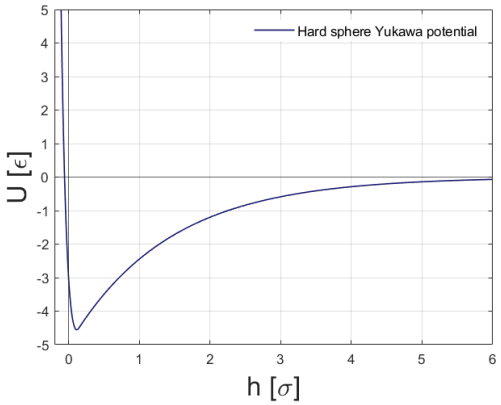

Figure 3.8: The hard sphere Yukawa potential. $\frac{1}{\kappa d} = 0.1$, $\kappa = 0.714$, and $A/\kappa = -5k_{\mathrm{B}}T$.

3.3.2 Yukawa interactions

In this research, the hard core Yukawa potential is used to investigate the effect of interactive particles. In LAMMPS, a Yukawa potential is available for finite-size spheres, named as pair style `yukawa/colloid`. The equation describing the potential is stated as

$$U_{\mathrm{Y}}(r) = \frac{A}{\kappa} e^{-\kappa(r-(a_i+a_j))}. \tag{3.10}$$

A is a measure of the interaction energy. The Yukawa potential can be used both as a repulsive and attractive potential. The sign of A indicates the type of interaction; negative values indicate attraction and positive values indicate repulsion. The range of attraction is the screening length κ^{-1}. A/κ is the value of the potential at contact and is used to indicate the strength of the interaction. To create the hard core Yukawa potential, the hard sphere potential has to be added to the potential in Equation 3.10. This is done with the pair style `hybrid/overlay`. The resulting hard-core potential is plotted in Figure 3.8 for the attractive Yukawa potential.

3.4 Ensembles

Classical molecular dynamics are energy conserving; potential energy is transferred to kinetic energy and the other way around; the sum always stays the same (Gallavotti, 1999). This does not mean that all particles in the system contain the same energy. The energy is distributed over the particles and is interchanged. With the same total energy, different states of the system exist. All these states together form an ensemble. In the case of energy conservation, the total energy (E) is constant. This ensemble is called the NVE ensemble. Two other parameters of the system also stay constant, namely the number of particles (N) and the volume (V). In experiments, it is hard to control energy; more often temperature and pressure are chosen as a constant. This results in a different collection of states of the system, and therefore a different ensemble. The ensemble for a constant temperature (T) is called an NVT ensemble and for a constant temperature and pressure (P) an NPT ensemble. Fixing the temperature can be physically interpreted by putting the system in contact with a reservoir with which it can exchange energy; this is called a thermostat (Frenkel and Smit, 1996). A barostat is based on the same principle, except that the volume of the system can also vary. Figure 3.9 gives a schematic representation of the NVT and NPT ensembles. In every ensemble, three parameters are varied to keep the others constant; for NVT [μ,P,E], for NPT [μ,V,E], and for NVE [μ,P,T]. The chemical potential (μ) is for all three ensembles constant. For large enough systems, all relative fluctuations are insignificant and all ensembles yield the same result. This is called the thermodynamic equivalence (Gallavotti, 1999). In this work, the focus lies on NVE and NVT ensembles. A constant volume is preferred to keep the volume fractions constant during the simulation.

There are several types of thermostats available in LAMMPS (Sandia Corporation, 2020). The Berendsen, Langevin en Nosé Hoover thermostat all control the temperature in their way. The Berendsen thermostat has of those thermostats the most apparent approach; rescaling of the velocity. The velocities are scaled at each step, such that the rate at which the temperature changes is proportional to the difference in temperature (Gallavotti, 1999). This method gives an exponential decay of the system towards the desired temperature (Frenkel and Smit, 1996). In the Langevin thermostat, all particles are corrected each time step by a random force and friction to lower their velocities (Grest and Kremer, 1986). The ratio between the force and the friction determines the temperature. The random corrections obey the fluctuation-dissipation theorem, thereby guaranteeing NVT statistics. The Nosé Hoover thermostat is the default thermostat of LAMMPS. It introduces a time stretch factor, which implies that if the instantaneous T is too low, the particles are accelerated or the clock is slowed down (Rühle, 2007).

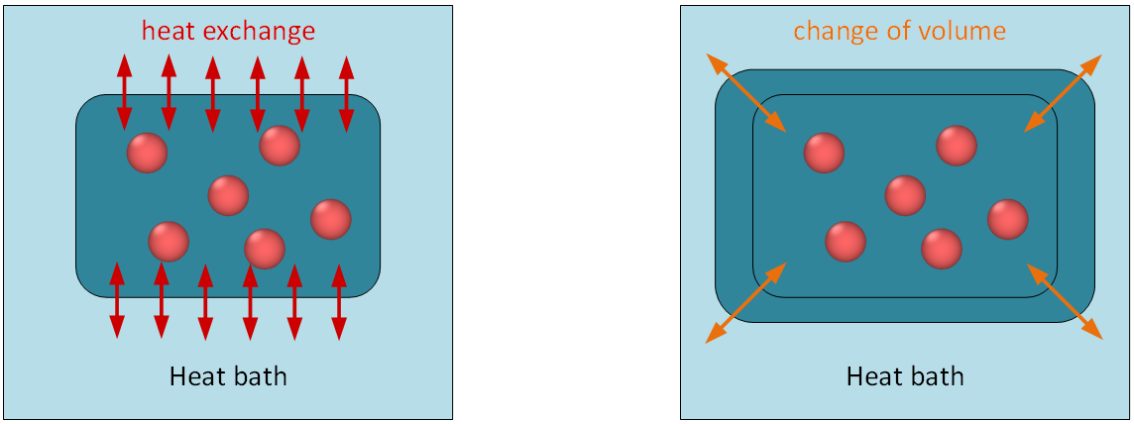

(a) NVT ensemble.

(b) NPT ensemble.

Figure 3.9: A schematical representation of the NVT and NPT ensemble.

3.5 Timestep analysis

The size of the timestep is of great importance in the fidelity of the simulations. However, there is a trade-off between this fidelity and the computation time when choosing the time step. The larger the timestep, the worse the conservation of energy throughout the simulation, which can lead to computational errors. It is therefore important to do a timestep analysis in which the energies in the system are evaluated. This analysis can best be done in the NVE ensemble. When the timestep dependency marginalizes, the timestep is appropriate. In Figure 3.10, such an analysis is done for a system containing 100 MHS particles. It becomes clear from Table 3.3 and Figure 3.10 that a step size of $0.01\,t^*$ is too big to simulate the energy accurately. It is decided that the standard deviation of magnitude 10^{-6}, corresponding to the step size $0.001\,t^*$, is small enough to work with.

Step size $[t^*]$	0.01	0.001	0.0001
Standard deviation $[\epsilon]$	1.23e-04	1.18e-06	2.74e-08

Table 3.3: The influence of step size on the standard deviation of the total energy.

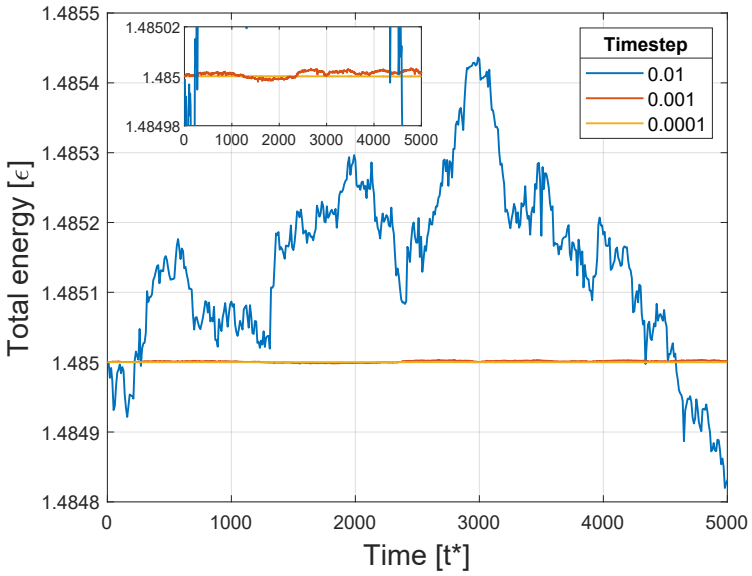

Figure 3.10: The effect of the size of the timestep on the total energy in the system. This system contains 100 MHS colloidal particles in a vacuum.

Chapter 4

Modeling the solvent dynamics

Accurate modeling of solvent effects is of great importance to develop simulations with a high fidelity. Solvent dynamics influence both mesoscopic phenomena (i.e. self-diffusion) and macroscopic phenomena (i.e. shearing, vorticity) in the system. Generally, colloidal particles show Brownian motion, which is caused by many random collisions with the solvent molecules. The colloidal particles are course grained in this model, but typically exist of millions, or even billions, of atoms (Frenkel and Smit, 1996). The amount of solvent particles around the particle is even more substantial, especially for diluted systems. The dynamics of the solvent are essential for the investigated phenomena, but the detailed properties are not of interest (Malevanets, 1999). There are two ways of modeling the solvent: explicitly and implicitly. In explicit methods the solvent molecules are modeled as individual particles. Not only the colloid-colloid pair interactions, but also the colloid-solvent and solvent-solvent interactions have to be computed every timestep. Therefore, the computation of the forces increased drastically in time. For a simulation containing only 12 `MHS` colloidal particles with a total volume fraction of 4 vol.%, a solvent volume density of 40%, and 1,000,00 timesteps, the number of explicit particles and the computation time is shown in Table 4.1. These simulations are, due to their long computation times, performed on a High Performance Cluster (HPC). This HPC has an Intel Xeon CPU (E5-2680 0) with 2.70 GHz and 64 GB RAM. The computation times can be brought down by reducing the number of particles, enlarging the timesteps, and reducing the cut-off ranges. However, in Chapter 3, it was shown that at least 1000 colloidal particles are required for useful statistics and that a step size of 0.001 is minimum for energy conservation. The cut-off range is already minimized in the performed simulations and would only extend for interactive particles. Accordingly, modeling the system with an explicit solvent is out of the scope of this project.

Particle size σ	14	16	18	20
Number of explicit particles	308,969	446,749	643,350	890,318
Computation time [days:hours:minutes]	3:16:07	5:17:12	8:20:10	12:23:06

Table 4.1: The computation time for a system containing explicit solvent particles. The simulation specifics are: 12 particles, 4 vol.% colloids, 40 vol.% solvent, 1,000,000 timesteps.

To reduce the computational demand, the solvent can be treated implicitly. This means that the solvent will no longer be modeled as individual particles, but rather as a continuous medium. The implicit model has to incorporate the essential dynamical properties of the solvent. The dynamics of interest often occur on long time and length scales. Not only the main dynamical features have to be reproduced, but also there has to be a microscopic coupling with the colloidal particles; e.g. when two particles collide this also affects the surrounding fluid flow (Malevanets, 1999). While fulfilling these requirements, the model has to be simple enough to run for long simulation times (Malevanets, 1999). The physical effects that are typically induced by the solvent can be modeled in several ways.

In this work, this is done with Langevin dynamics. Using an implicit solvent in the model seems very obvious. However, in coagulation, external forces play a crucial role. These forces are not straightforward to combine with the implicit method. Chapter 6 focuses on the effective modeling of shear forces while using an implicit solvent.

4.1 Langevin dynamics

The Langevin thermostat is already briefly introduced in Chapter 2. The thermostat is based on Langevin dynamics. These dynamics let the colloids act as Brownian particles, without explicitly taking the solvent molecules into account. The dynamic equations include stochastic forces that mimic the solvent effects (F_f en F_r), in addition to the systematic conservative forces between the colloidal particles (F_c)(Schlick, 2010).

$$F_{\text{Langevin}} = F_c + F_f + F_r \tag{4.1}$$

F_f represents the force caused by frictional drag, proportional to the particle velocity. F_r is a force due to solvent atoms randomly bumping into the particle (Sandia Corporation, 2020). From classical Brownian theories, it appears that while the molecular collisions are random, all solvent molecules together produce a systematic effect (Schlick, 2010). The frictional force and the random force are related by the fluctuation-dissipation theorem (Kubo, 1966). This theorem states that the dissipative force is related to the variance of the random force (Schlick, 2010). This results in Equations 4.2 and 4.3:

$$F_f = -\frac{m}{\gamma} v \tag{4.2}$$

$$F_r \propto \sqrt{\frac{k_B T m}{\mathrm{d}t\ \gamma}} \tag{4.3}$$

It is important to scale the mass, m, with the size of the colloidal particles, since the mass influences both the friction and random solvent forces. The damping constant, γ, is the critical parameter in the equations. It determines the relative strength of the friction forces with respect to the random forces. The damping constant determines how rapidly the temperature is relaxed in the Langevin thermostat and therefore is specified in time units. An ample relaxation time time implies a low viscosity solvent (Sandia Corporation, 2020).

The disadvantage of Langevin dynamics is that they do not take hydrodynamic forces into account. Hydrodynamic forces arise when there are multiple colloidal particles in a system. The motion of one particle induces a flow field in the fluid that alters the friction felt by other particles (Gompper et al., 2009). The hydrodynamic interactions can be felt between particles, even if the particles are far apart from each other; the flow fields decay very slowly over distance. Therefore, the volume fraction of colloids has to be very low to neglect the hydrodynamic interactions (Padding and Louis, 2006). Also at very high colloid volume fractions, the direct particle interactions dominate the hydrodynamic interactions, and therefore the hydrodynamic interactions can be neglected. The required volume fraction for this to happen depends on the cut-off range of the pair potentials (Padding and Louis, 2006); the larger the range, the lower the required volume fraction. This means that for hard sphere particles, which have an interaction range equal to zero, the hydrodynamic forces always stay dominant. At very high volume fractions, where particles almost reach their maximal packing, the hydrodynamic forces become lubrication forces. Lubrication forces are associated with squeezing a fluid in and out of a region between two particles. The implicit Langevin model is known for its simplicity and, therefore, favorable in use. Since it does not take the dynamics into account, the method is especially useful for studying equilibrium properties (Wang et al., 2016). Although in this work a non-equilibrium model is developed, the Langevin method is chosen to model the solvent dynamics. Other more extensive methods often take Langevin dynamics as the basis for the solvent dynamics and extend the method to include the hydrodynamic properties (Wang et al., 2016). A thorough understanding of the Langevin dynamics in equilibrium situations contributes to a good foundation of the coagulation model. In a later stage, the model can further be developed to include hydrodynamic forces. This can

be done with the SELM software package, which can be implemented in LAMMPS(Wang et al., 2016). The limitations of the Langevin method are kept in mind during this study.

4.2 Tuning the solvent dynamics

The solvent dynamics of the model are validated based on the diffusive behavior of the colloids. In the dilute regime, the colloidal particles undergo Brownian motion. As explained in Chapter 2, the self-diffusion coefficient and the particle radius are inversely proportional when following the Brownian behavior. The mean square displacement does not only provide the diffusion coefficient, its characteristic shape is also an indication of Brownian motion. A specific solvent condition is simulated for four particle sizes; 14, 16, 18, and 20 σ. The mutual diffusion coefficient ratios are compared to the inverse size ratio. This gives a percentile deviation for every size pair. The average of all the percentages can be calculated. This average indicates how close the particle behavior is to Brownian motion. Beneath a small example is given for diffusion coefficients $D_{14} = 139D^*$, $D_{16} = 127D^*$, and $D_{18} = 113D^*$. In further results, only the average deviation, in this case 3%, will be mentioned.

	14/16	14/18	16/18
Inverse ratio size	1.143	1.286	1.125
Ratio diffusion coefficient	1.092	1.237	1.133
Percentile deviation	4.5%	3.8%	0.7%
Average deviation	3.0%		

Table 4.2: The calculation of the simulation accuracy. In the example, the system contains 4 vol.% colloidal particles and the damping constant is set to be $1000t^*$.

The Langevin solvent dynamics can be tuned with the damping constant, γ. The first exploration of γ is performed in simulations containing 1000 particles with a volume fraction of 0.04. The results are listed in Table 4.3. As the damping coefficient increases, the diffusion of the colloids starts to be comparable to the Brownian diffusion. What is also interesting to see is the trend of the mean square displacement at the smaller timescales (Figure 4.1). Both systems show a ballistic regime in their mean square displacement. However, the timescale at which this regime is located is very different. A low γ means a high viscosity. High viscosity systems are dense systems; the particles experience the friction by the solvent at a shorter time scale. This matches the behavior in Figure 4.1.

A first indication is obtained for the magnitude of γ. Next, the solvent dynamics can be further optimized. Both the Brownian behavior as the Langevin dynamics work best in the diluted regime. Therefore the optimization is done in a more diluted system of 1 vol.%. In the optimization, γ is further increased. The results are listed in Table 4.4. For a smaller volume fraction of the particles, it appears that the damping constant even has to be higher to resemble the Brownian dynamics. The optimal behavior is found at $\gamma = 7500t^*$. Using this value for simulations of 4 and 7 vol.% gives average deviations of respectively 2.0 and 8.1%. The higher value for the 7 vol.% system is expected since the deviation of an ideal system becomes bigger. A colloidal volume fraction of 4 vol.% is small enough to let the particles behave as the desired Brownian particles. The relationship between diffusion coefficients for systems of different colloidal volume fractions is also evaluated. It is expected that the smallest volume fraction has the highest diffusion coefficient, as is stated in Equation 2.6. This relationship is valid for the obtained data. In Figure 4.2, the mean square displacements are shown for the optimized system. In this graph, the standard deviation is indicated. The deviation shows the effect of using different random seeds in the model. The further the mean square displacements proceed in time, the higher standard deviation of the model. However, the average standard deviation of all simulations is merely around 2%.

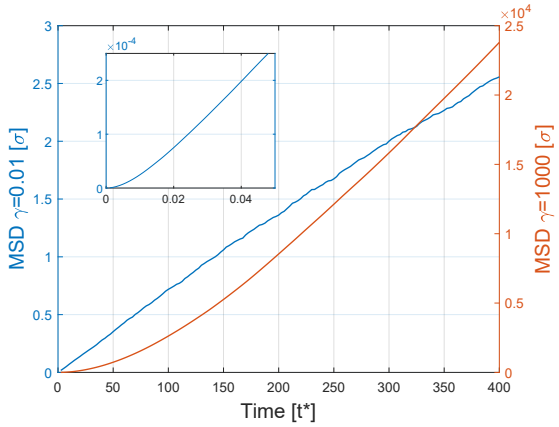

Figure 4.1: The mean square displacement at small timescales for a simulation with $\gamma = 0.01t^*$ and $\gamma = 1000t^*$. The results are for a 4 vol.% system with particles of 14σ.

$\gamma\,[t^*]$	Average deviation of the Brownian behavior
0.001	52.0%
0.01	25.7%
1	47.7%
100	33.8%
1000	2.5%

Table 4.3: The deviation of the typical Brownian particle behavior based on the damping constant, γ. The system contained 1000 colloidal particles with a density of 4 vol.%.

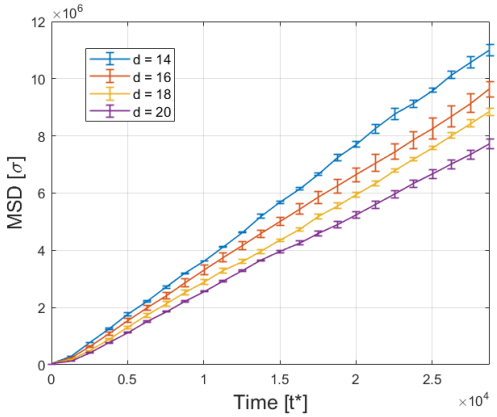

Figure 4.2: The mean square displacement for a system with the best solvent dynamics at 1vol.%.

$\gamma\,[t^*]$	Average deviation of the Brownian behavior
1000	21.9%
2500	6.0%
5000	4.3%
7500	3.0%
10000	8.4%

Table 4.4: The deviation of the ideal Brownian particle behavior based on the damping constant, γ. The system contained 1000 colloidal particles with a density of 1 vol.%.

4.3 Beyond the hard sphere particle interactions

With the solvent dynamics that are defined in the previous section the diffusive behavior of the colloidal particles can be further explored. All previous simulations are performed with hard sphere particle interactions. In this section, the interactions are extended beyond the hard sphere range. This is done with the hard sphere Yukawa (HSY) potential, see section 3.3.2 for the implementation in the model. The potential is characterized by two properties: the strength of the interaction at contact (A/κ) and the range of interaction ($1/\kappa d$). Figure 4.3 shows the effect that interactions have on the diffusive behavior. As expected, the diffusion coefficient decreases. With a repulsive interaction, the excluded volume of the particles increases, thus the effective volume fraction increases. As was shown previously, the mean square displacement decreases with a higher volume fraction. With an

attractive interaction the particles are even more constrained in their motion. The probability that two particles are closely together becomes larger due to the attractive potential. The chance on collisions therefore increases, thus the diffusion decreases. Additionally, the proximity of other particles induces additional hydrodynamic interactions, which increase the effective friction (Dhont, 1996). A more sophisticated implicit method could, therefore, even give a lower diffusion of the attractive particles.

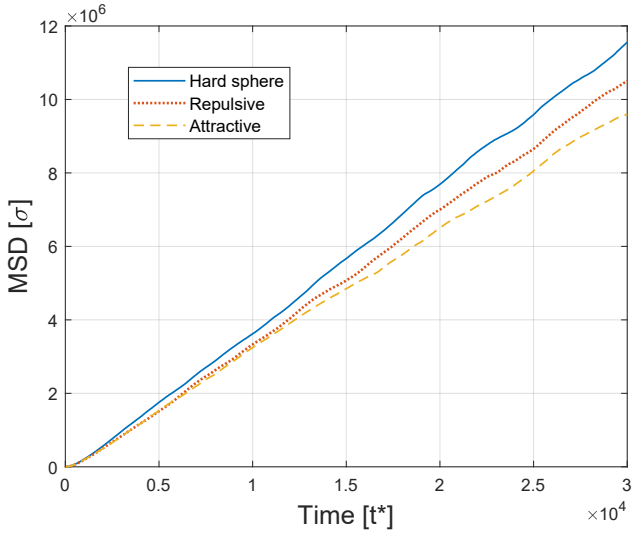

Figure 4.3: The effect of interactions on the mean square displacement. The simulations are performed with $\gamma = 7500\,t^*, d = 14$, and 1 vol.%. The repulsive and attractive potentials have a strength of respectively 5 and $-5k_BT$ and a range of 0.05.

4.3.1 Size dependence

Comparing Equation 2.8 and 2.9 shows that the diffusion coefficient is now depending on the extra property τ. This stickiness parameter can be calculated with the second virial coefficient. Which in turn depends on the interaction potential, see Equation 2.10 and 2.11. The stickiness parameter is calculated for the attractive HSY potentials. The particle size is varied, but the range and strength of the interaction are kept constant, resulting in the same τ for every particle size. The constant τ means that the ratio in diffusion coefficients is still only depending on the particle size, as described in Equation 2.7. The deviation of the expected particle behavior is again measured by comparing the actual ratio to the expected ratio. Table 4.5 shows that the deviation of the ideal behavior increases with the increasing range of interaction. The increase is most significant for the attractive interactions, which can be an indication that the lack of hydrodynamic interaction is the most important reason for the bigger deviation.

4.3.2 Interaction range dependence

While changing the size does not affect the stickiness parameter, changing the interaction range does. In the following results, the size of a particle is kept constant and the range of interaction is varied. Since τ is no longer a constant value, the deviation can no longer be calculated by simply looking at the ratio of diffusion coefficients and particle sizes. Equation 4.4 shows the proportional relation between the diffusion coefficient and the stickiness parameter,

$$D_s^L \sim \frac{\tau - 2.0972\phi\tau - 0.562\phi}{\tau}. \tag{4.4}$$

	Attractive	Repulsive
HS	3%	
range 0.05	4.1%	4.7%
range 0.1	9.1%	6.4%
range 0.15	10.7%	8.8%
range 0.20	11.1%	6.8%

Table 4.5: The average percentile deviation of the Brownian behavior. The simulations are performed for both attractive and repulsive interactions at different ranges of interaction. The system is defined with γ is 1000 and the colloidal fraction is 1 vol.%.

The average deviation in Table 4.6 is calculated for six different ranges at every colloidal size; $\frac{1}{\kappa d} = 0.02$, 0.05, 0.07, 0.1, 0.15, and 0.2. Relation 4.4 is used to calculate the theoretical ratios. The theoretical ratios are again compared to the ratios obtained from the simulation data. The average deviation of the expected behavior is above 40%, which means that the model would not be able at all to take the interaction range into account. However, taking a closer look clarifies the behavior. The relationship for τ is derived by Baxter (1968) for sticky spheres. In his model, the attractive well is infinitely small. Regnaut and Ravey (1989) investigated the possibilities to extend the sticky sphere model to larger ranges of attraction. He found that beyond a range of 0.1 the model is no longer capable of accurate predictions. In the third column of Table 4.6, the average is calculated with ranges higher than 0.1 excluded, which resulted in much better results. The magnitude of the deviation is now of the same magnitude as it was in Table 4.5. A possible cause of these deviations are the hydrodynamic forces that are not taken into account.

Particle size	Average deviation	Average deviation for $\frac{1}{\kappa d} < 0.1$
14	40%	13%
16	41%	11%
18	51%	17%
20	41%	13%

Table 4.6: The average percentile deviation of the Brownian behavior. The simulations are performed for both attractive interactions at different particle sizes. The system is defined with γ is 1000 and the colloidal fraction is 1 vol.%.

The effect of attraction on the behavior of the particles can also be quantified with the radial distribution function $g(r)$. Figure 4.4 shows the radial distribution function for a system containing particles with a diameter of 14σ, 1 vol.%, and $\gamma = 7500t^*$. Two things are notable in the figure. First of all, there is no second peak at r/d=2, which means only pairs of atoms are sticking together. This can be explained by the low volume fraction. The chance that two particles encounter each other is small, let alone that three particles do. Secondly, the height of the peaks at r/d=1 does not scale with the range of attraction. The peak height increases until the range of 0.07 and after that it starts decreasing again. The radial distribution function of the simulations is calculated in histogram form by binning pairwise distances into $Nbin$ bins from 0.0 to a defined cut-off distance (Sandia Corporation, 2020). In Figures 4.4a and 4.4b the cutoff distance is varied, while the number of bins is kept constant, $Nbin = 150$. The difference between the two figures shows the significant effect that binning has on the radial distribution function.

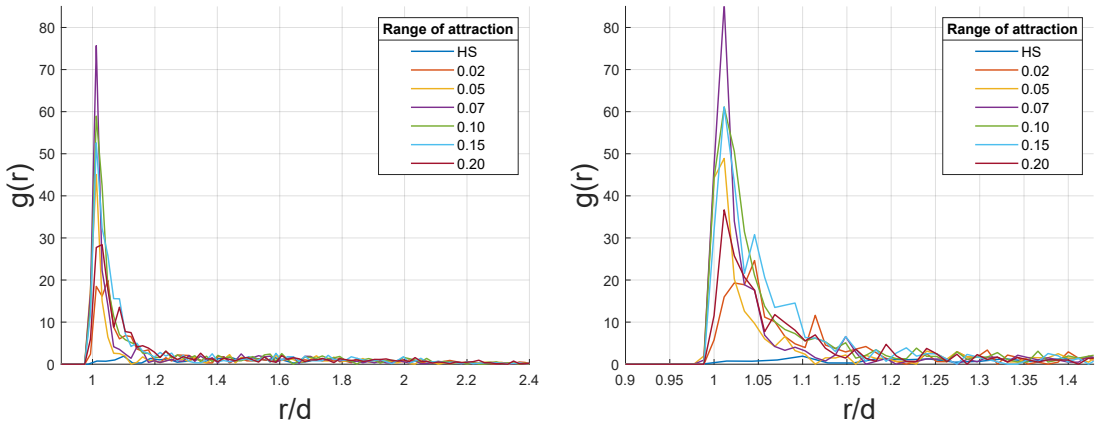

(a) Larger radial distances. Binsize = 0.019.

(b) Smaller radial distances. Binsize = 0.011.

Figure 4.4: The simulated radial distribution function.

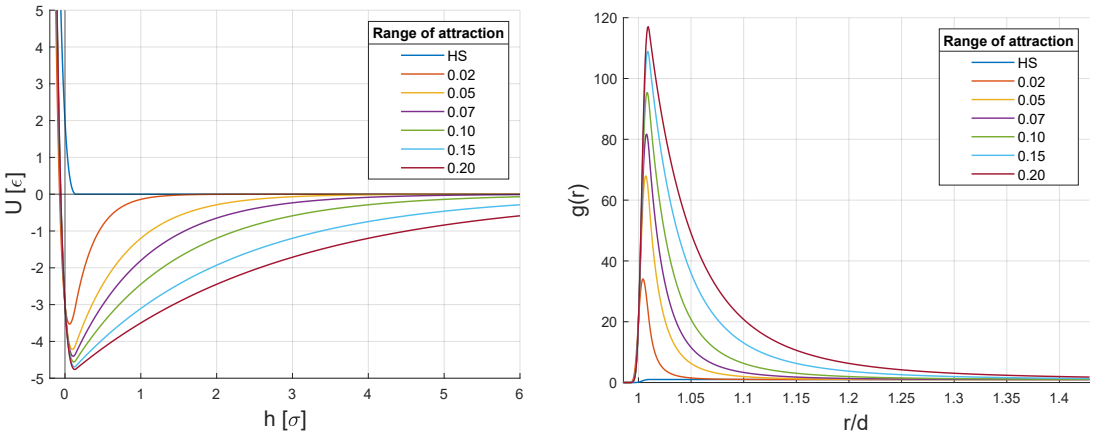

(a) Interaction potential.

(b) Radial distribution function.

Figure 4.5: The effect of the interaction range on the theoretical radial distribution function and the interaction potential for a system containing hard sphere Yukawa particles.

The theoretical radial distribution function in the diluted regime can be described by

$$g(r) = \exp(-U(r)). \tag{4.5}$$

Figure 4.5 shows respectively the HSY potentials and the corresponding theoretical radial distribution functions. Binning of the theoretical radial distribution function slightly lowers the peak height, however, the overall shape and peak order stays the same. Appendix D shows the binned graph and also shows a graph in which the data of the simulated and theoretical radial distribution function are plotted simultaneously. With this in mind, a fair comparison can be made between the theoretical and simulated radial distribution function. The peak heights for interaction ranges below 0.1 are approximately the same. It appears that for interaction ranges $\frac{1}{\kappa d} \geq 0.1$ the system shows a divergence from the expected behavior.

A colloidal system of at least 1000 particles is required for useful statistics. The use of the implicit Langevin solvent contributes to the development of a model that can efficiently model these large colloidal systems. A damping constant of $7500\,t^*$ is required to accurately simulate the behavior of

colloidal particles in dilute systems. For interactions beyond the hard sphere regime, the deviations of the model slightly increase, by lack of hydrodynamic forces. These solvent settings are maintained during the further proceeding of this work.

Chapter 5

Polydispersity

In previous chapters, simplifications are applied to the emulsion polymerization system to create an efficient model. Only the components of the colloidal scale are explicitly modeled. In Chapter 2, the crucial mechanics and interactions for coagulation are discussed. Contradictory, the small components that had to be neglected for computational efficiency (micelles, polymer chains, and monomers), can play a role in coagulation. Because of the size difference, an effective attractive force can be induced by the small particles, the depletion force. The particles inducing the force are called depletants. In this chapter, it is discussed how to incorporate the depletion forces in the model while keeping the efficiency high.

In this study, the depletants are seen as hard spheres, which is an accurate representation in case the depletion forces are induced by other colloidal particles; the monomer droplets and the polymer particles. If the polymers in the solution cause the depletion interaction, penetrable hard spheres would be a better representation of the depletants (Lekkerkerker and Tuinier, 2011). The depletion potential between two colloidal spheres due to smaller hard spheres is described as

$$U_{\text{depl}} = \begin{cases} -\frac{a}{d_d}[3\phi_d\lambda^2 - \frac{\phi_d^2}{5}(12-45\lambda-60\lambda^2] & 0 \le h < d_d \\ \frac{a\phi_d^2}{5d_d}[12-45\lambda+60\lambda^2-30\lambda^3+3\lambda^5] & d_d \le h < 2d_d \\ 0 & h \ge 2d_d \end{cases} \tag{5.1}$$

In this equation, ϕ_d is the volume fraction of the depletants, a is the colloidal radius, and d_d is the depletant diameter. A measure of the inter-particle distance is λ, which is equal to $(h-d_d)/d_d$. The strength and range of the interaction can be tuned with the depletant concentration and with the depletant-to-colloid ratio (González García and Tuinier, 2016). The depletant-to-colloid ratio is defined as $q = d_d/2a$. The effect of these parameters is shown in Figure 5.1. To prevent overlap of multiple depletion zones the diameter of the colloidal particles needs to be at least seven times bigger than the diameter of the depletant particle, which means that $q < 0.15$. For small q's the potential is pairwise additive (González García and Tuinier, 2016). Dijkstra (Dijkstra et al., 2006) showed that for size ratios of $q = 0.1$ the number of overlapping of depletion layers is no larger than 2. For $q = 0.6$, the number of overlapping layers can go up to 7, depending on the colloid packing fraction.

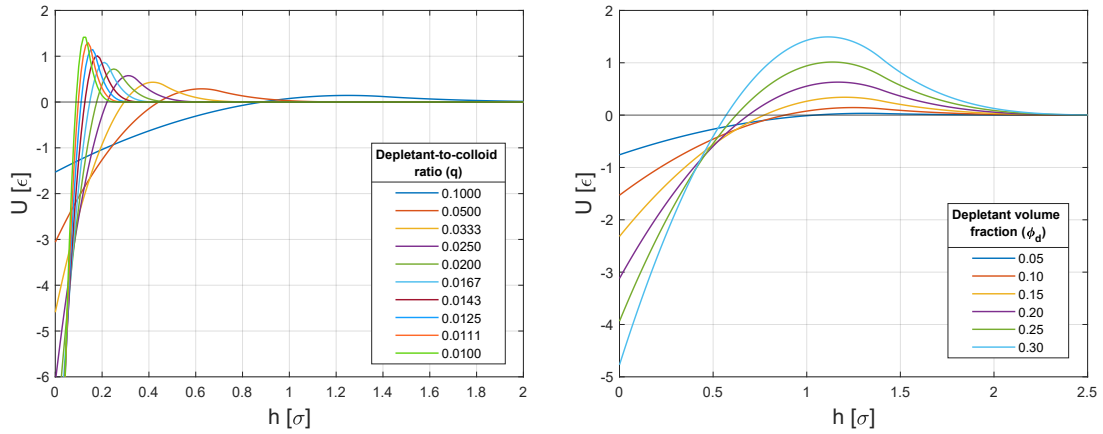

(a) Effect depletant-to-colloid ratio. $\phi_d = 0.1$.

(b) Effect depletant volume fraction. $q = 0.1$.

Figure 5.1: The depletion potential can be tuned by varying the depletant-to-colloid ratio and the depletant volume fraction.

5.1 Explicit depletant particles

The simplest method to introduce depletion forces is simply adding depletant particles to the system. To have a fair comparison between the different depletion potentials the interaction strength at contact is set on a constant value of $-5k_BT$. The same interaction strength was set for the hard sphere Yukawa potentials in Chapter 4; this makes the results easy to compare. For a known depletant-to-colloid ratio, the required depletant volume fraction can be calculated by

$$U_{\text{depl},(h=0)} = -3\frac{a}{d_d}\left(\phi_d + \frac{1}{5}\phi_d^2\right). \tag{5.2}$$

In Table 5.1, the depletant properties are listed for different colloid-to-depletant size ratios. The smaller the depletant particles, the smaller the volume fraction that is required for the same interaction strength. While the volume fraction is decreasing, the number of depletant particles increases drastically. Even for depletant particles that are only ten times smaller in size, already 31 million depletant particles are required. Unfortunately, modeling such a large number of particles requires enormous amounts of computational power, which is beyond the scope of this work.

depletant-to-colloid ratio (q)	0.1	0.02	0.01
Depletant volume fraction	0.314	0.066	0.033
Maximum value of the potential $[k_BT]$	1.75	0.33	0.15
Number of depletant particles (for a system with 1000 colloidal particles and 1 vol.%)	31,365,717	822,508,997	3,311,402,560

Table 5.1: An overview of the depletant properties corresponding to a depletion potential with a contact strength of $-5k_BT$.

5.2 Reproducing the depletion potential

It is not practical to induce the depletion potential explicitly. The same limitations are experienced as for modeling the solvent dynamics. The solvent dynamics are now incorporated by inducing the average solvent force on the colloidal particles. A similar approach can be taken to induce depletion

forces. However, the depletion forces are depending on the inter-particle distance, thus have to be modeled as an additional pair potential. Unfortunately, LAMMPS does not contain a pair style that directly represents the depletion potential. However, several Yukawa potentials can be combined to reproduce other potentials. The number of Yukawa potentials that are summed is referred to as the number of Yukawa tails. The values for the A's and κ's determine the shape of the n-tails Yukawa potential.

$$U_{Y_{\text{n-tails}}} = \frac{A_1}{\kappa_1}\exp(-\kappa_1 h) + \frac{A_2}{\kappa_2}\exp(-\kappa_2 h) + \cdots + \frac{A_n}{\kappa_n}\exp(-\kappa_n h). \tag{5.3}$$

In this work, two methods are provided to fit the n-tails Yukawa potential (Equation 5.3) to the effective depletion interaction (Equation 5.1). These methods differ in their fitting procedure. The root finding method requires a number of equations equal to the number of variables that have to be solved and searches for a numerical solution to the simultaneous equations. The least-squares minimization method subtracts the depletion potential and n-tails Yukawa potential and searches for the minimum difference. The fitting takes place in Mathematica.

5.2.1 Root finding method

The root finding method makes use of four equations that describe a particular aspect of the depletion potential, listed below. The four equations can be used to fit an equal amount of parameters. Since every Yukawa potential contains two variables (the reciprocal screening length κ and the force strength A), a 2-tails Yukawa potential can be used in the fitting. The inter-particle distance is given in a reduced unit, $\tilde{r} = r/2a$.

- The second virial coefficient (González García, 2019)

$$\frac{B_2}{v_c} = 4 + 12\int_{\tilde{r}=1}^{\tilde{r}=\infty} 2\pi\tilde{r}^2\left(1-\exp\left[-U\left(\tilde{r}\right)\right]\right)d\tilde{r}. \tag{5.4}$$

- The area under the graph

$$A = \int_{\tilde{r}=1}^{\tilde{r}=\infty} 4\pi\tilde{r}^2 U(\tilde{r}) d\tilde{r}. \tag{5.5}$$

- The potential at contact

- The maximum value

These four aspects should be exactly equal for the depletion potential and the two tail Yukawa potential (González García, 2019). The initial values of the Yukawa parameters have a significant impact on the final result. These can be guessed by first fitting a 1-tail Yukawa potential, which indicates the magnitude of the variables. Moreover, it is important that the pre-factors, $\frac{A}{\kappa}$, of the two Yukawa potentials together are approximately equal to the contact potential of the depletion potential. The limitation of this method is the number of Yukawa tails that can be fitted. On the other hand, the computing time is fast. Furthermore, for depletion potentials with low volume fractions, thus with a low repulsive barrier, a good fit can be achieved. Figure 5.2a shows a fit for a very low depletant density. For the potentials with a low repulsive barrier, the use of the second virial coefficients as one of the fitting constraints is also an advantage. Noro and Frenkel (Noro and Frenkel, 2000) found that the potentials with the same reduced virial coefficient have the same effective range of attraction. This is called the extended law of corresponding states. This law is particularly applicable to entirely attractive potentials. For potentials that contain a repulsive barrier, they found deviations from the extended corresponding states behavior.

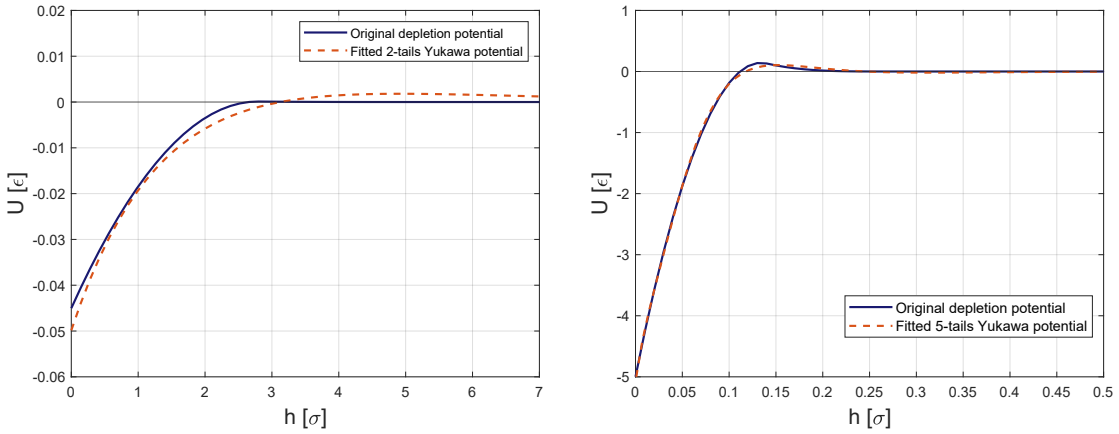

(a) Root finding method. For q=0.1 and $\phi_d = 0.003$.

(b) Minimization method. For q=0.01 and $\phi_d = 0.0331$

Figure 5.2: The n-tails Yukawa potential fitted by the root finding and least-squares minimization method.

5.2.2 Least-squares minimization method

The least-squares minimization method only requires the equations that describe the depletion and n-tails Yukawa potential. The difference between the potentials is minimized by varying the Yukawa parameters. The standard deviation expresses the final accuracy of the fit. The lower this value, the better the fit. The minimization can be performed via different procedures. These procedures are shortly explained in Appendix E. In this appendix a table is appended that lists the standard deviation and computation time for different number Yukawa tails. While the computation times are the longest, the standard deviations of the RandomSearch method are by far the smallest. The method performs better since it prevents to get trapped in a local minimum. The standard deviation for an increasing number of Yukawa tails is shown in Table 5.2. A lower number of tails is preferred for modeling efficiency. The improvement that can be gained on the standard deviation decreases with an increasing number of tails; the standard deviation decreases with 22% going from 4 to 5 tails, while it decreases less than 5% going from 5 to 6 tails. Therefore, the 5-tails Yukawa potentials are chosen to reproduce the depletion potential. Also, Table 5.2 and Figure 5.3 combined, show that it becomes harder to fit the potential, when the repulsive barrier is more prominent. The obtained 5-tails Yukawa parameters are listed in Appendix F. In the same appendix, the 5-tails Yukawa potentials are plotted together with the corresponding depletion potential.

Depletant-to-colloid ratio (q)	**2-tails**	**3-tails**	**4-tails**	**5-tails**	**6-tails**
0.1	0.140	0.078	0.054	0.042	0.040
0.02	0.078	0.039	0.026	0.020	0.019
0.01	0.055	0.032	0.020	0.016	0.014

Table 5.2: The standard deviation in ϵ depending on the number of Yukawa tails.

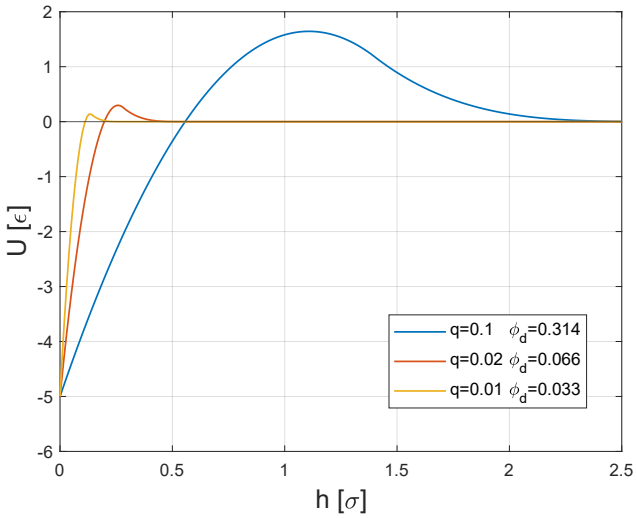

Figure 5.3: The depletion potential for an interaction strength of $-5k_BT$.

5.3 Simulating the Yukawa depletion potential

LAMMPS allows for the summation of multiple potentials with the pair style `hybrid/overlay`. This pair style is been used to plot the HS potential and 5 Yukawa potentials for the pair interaction between the colloids. However, running the model gives an error after a certain amount of time steps; Lost atoms. This error often occurs when particles have a substantial overlap, which causes a high particle energy and infinitely high forces. This makes the particle 'shoot' through the system. To test whether the particle collisions are indeed the cause of the error, the initial position of the particles is altered. Indeed, the system crashed after far more timesteps when the particles are placed further apart. Furthermore, the step size is decreased to see whether the steepness of the potential plays a role. However, around the same simulation time, the program stops. This means that when LAMMPS tries to stack the potentials something goes wrong. It can be that LAMMPS has a limit in the amount of Yukawa potentials that can be stacked. This has to be further investigated.

Fitting the depletion potential with the n-tails Yukawa potential is one method to produce the depletion potential in LAMMPS. Another possibility is to create a new pair style, as is done for the hard sphere approximation. The advantage of an implemented pair style is that there is no additional software required for the fitting, furthermore, the potential is exact and not an approximation. However, using already existing LAMMPS pair styles is often preferred. The already implemented pair styles are approved by the authors of LAMMPS, which means that they are fully complementary with the rest of the code. Newly created pair styles require much validation, as is done for the `MHS` pair style.

Like the depletants induce depletion forces, there are more phenomena of smaller length scales that can induce effective potentials between the colloidal particles. For example, repulsive solvation forces are induced by the interaction of lyophilic particles with the solvent. For an implicit solvent, these forces are not implemented. Moreover, steric repulsion is induced by polymer chains attached to the particles. It is computationally expensive to simulate these chains and their behavior explicitly. Hence, the methods discussed above have a more comprehensive application than just depletion interaction.

Chapter 6

Shear

Shear stresses are developed due to particles in the fluid moving with different velocities. Especially in tubular reactors, shear forces play an essential role since the surface-to-volume ratio is relatively high. Shear often arises at walls. The solvent particles have an interaction with the wall and therefore adopt the same velocity, which induces the velocity differences causing the shear stresses. It is clear that shear forces are transferred via the solvent particles. This imposes a challenge. An implicit solvent does not contain explicit solvent particles that can transfer the shear stress over the system. The interactions between the solvent and the colloidal particles are induced by stochastic forces. The methods that are implemented in LAMMPS do not take shear into account in these forces. This chapter starts with an introduction to the relevant theory on the effect of shear on colloidal systems. Subsequently, several methods are discussed to apply shear on the system.

When a stationary shear flow is applied, the system is no longer in equilibrium. There arises a competition between diffusion and shear effects, which together result in a new anisotropic microstructure. When diffusion is very fast, the microstructure is little affected. However, the equilibrium is disturbed in case the shear flow velocity is large(Dhont, 1996). The ratio between shear and diffusion in one dimension can be described with the Peclet number and is an estimate for the amount of distortion (Cheng et al., 2018).

$$\mathrm{Pe} = \frac{3\pi\mu G\, r_i\, r_j (r_i + r_j)}{2 k_B T}. \tag{6.1}$$

In this equation, G is the shear rate. The shear rate is equal to the velocity gradient that is induced by the shear stresses. When $\mathrm{Pe} \ll 1$, the particles are driven by their diffusion. When $\mathrm{Pe} \gg 1$, the particles are driven by flow.

The shear that is desired in the simulations is a simple shear flow, which means that the fluid velocity gradient is linear, as depicted in Figure 6.1. Only the upper wall moves, with a velocity V at height L. No-slip boundary conditions are assumed. Which means that the solvent layer at the wall adopts the velocity of the wall. The values for V and L in the model are respectively $2v^*$ and 524σ.

In the implementation of shear forces in LAMMPS, recalculation of the temperature is essential. The Langevin thermostat computes the temperature based on the velocities of the particles. Due to the imposed shear forces, the particles have high velocity in the x-direction. However, this velocity has nothing to do with the temperature of the system. With the `compute temp/ramp` command, a ramped velocity profile is subtracted of the velocities in the x-direction before computing the kinetic energy.

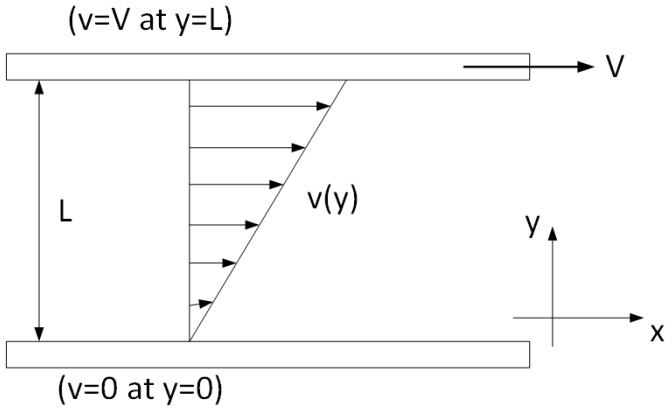

Figure 6.1: The linear velocity profile induced by a moving wall.

6.1 Moving rough wall

The first method that is suggested, is based on the conventional way of imposing shear. Walls are defined in the y-dimension and the upper wall moves with a velocity V in the x-direction, the other dimensions still contain periodic boundaries. Two wall types can be implemented in LAMMPS; rough and ideal walls. Rough walls consist of explicit wall particles. These particles are generated like any other particle. They can be constrained to a specific region, and by packing them closely, they act as a solid wall. The interactions between the mobile particles and the wall are set the same way as other particle interactions are set, with pair styles. To decrease computation power, the interactions between the wall particles are turned off. This can be done with the `neigh_modify exclude` command. Ideal walls are smooth walls placed on the surface of the indicated dimension. The interaction with the ideal walls is set in the `fix wall` command. In this command, also the wall interaction is defined. Because of the explicit character of the rough walls, a uniform movement can be assigned to the wall particles. This is done by first setting all forces on the wall particles equal to zero with the `fix setforce` command. Subsequently, the desired velocity can be defined with the `velocity set` command. For moving walls, it essential that the packing of the wall fits precisely within the box boundaries. This prevents an 'atoms lost' error. The disadvantage of rough walls is the number of particles in the simulations. A system containing 1000 colloidal particles of size 14σ at 1 vol.% already requires 549152 particles at one wall side. Despite the turned-off wall-wall interactions, the computation time increases drastically for rough walls.

Figure 6.5a shows the rough moving wall method. The interaction between the moving wall and the mobile particles has to be attractive to induce a shear force. Therefore, the hard sphere Yukawa potential is used to describe the interaction in these simulations. The range is set on 0.1 and the attraction strength on $-5k_{\mathrm{B}}T$. Figure 6.2 shows the velocity profile of the colloidal particles in the x-direction for different simulation times. The particles have a random velocity around zero. Even at height L there is no increased velocity. This means that there is full slip behavior at the wall. This is the result as expected. The moving wall is only for short moments within the interaction range of the particles. After the collision, the effects of the wall collision quickly fade away. Furthermore, the density of the particles is not high enough to pass across the momentum that is induced by the wall.

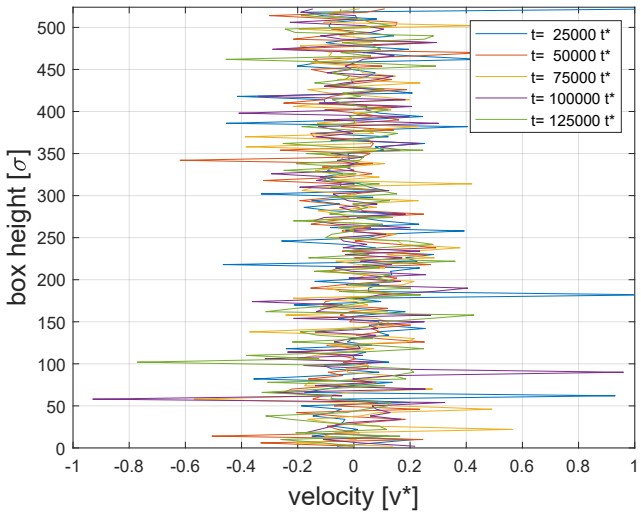

Figure 6.2: The velocity profile in the x-direction for the rough moving wall method.

6.2 External force

As is shortly explained in Chapter 3, external forces can be added to the system. This can be done on individual particles or a group. It is possible to exercise the force every timestep or with an interval. These additional forces can be used to replace the forces that arise from the flow of solvent. The Brownian particles immersed in the solvent do no longer feel the friction force, as described in Equation 4.2. Instead of the absolute velocity of the particle, the velocity is now defined as the difference of the local fluid and particle velocity (Dhont, 1996). The new friction force becomes,

$$F_f = -\frac{m}{\gamma}(v - v_f). \tag{6.2}$$

The friction force, as implemented in the Langevin dynamics, only involves the particle velocity v. The additional force, therefore, has to exercise a force, $F_{\text{add}} = \frac{m}{\gamma} v_f$. To create the linear velocity profile, the fluid velocity, v_f, is equal to

$$v_f = \frac{y}{L} V. \tag{6.3}$$

In this equation is y the position of the particle in the y-dimension. The additional force is imposed on all colloidal particles at every time step.

The first simulation with the additional force is performed in a simulation box containing periodic boundary conditions in all directions. Figure 6.3a shows the velocity profile for this simulation. The force clearly accelerates the particles in the x-direction. However, due to the boundary conditions the average x-velocity stays constant over the height of the box. To prevent the transfer of particles with a high x-velocity to the low-velocity regions, walls have to be implemented. The second simulation contains an ideal wall both at the upper and lower edge of the y-dimension, see Figure 6.5b. The ideal wall is computationally much more efficient, but does not have the ability to move. The wall can be implemented with the `fix wall` command. In total there are eight different fix wall commands. Each command specifies another interaction potential between the particles and the wall (Sandia Corporation, 2020). Non-interacting walls can be used since the walls do not have the shear inducing function. The command `fix wall/reflect` flips the sign of the corresponding velocity component, when a particle moves outside the wall. Figure 6.3b shows the corresponding velocity profile. The gradient of the profile becomes more apparent over time. After a time of $200,000t^*$, the profile has reached its steady shape. The profile shows a simple shear flow. However, the gradient is

not as high as desired. The maximum velocity reaches the velocity of $2v^*$, even slightly exceeds it. The minimum velocity, however, is supposed to stay around a velocity of $0v^*$. To slow down the particles at the lower regions, an attractive wall is placed at the lower y-edge. The interaction is defined as the 9,3-Lennard-Jones potential. This is one of the predefined ideal walls of LAMMPS. The profile in Figure 6.3c shows that the attractive wall does not slow down the particles at the lower regions compared to Figure 6.3b. The same as for the rough walls, the colloid particle wall interactions appear to have no significant effect. The low volume fraction of the colloids is the most probable cause of this. The effect of the particle wall interaction is likely to increase for higher densities and stronger interaction strengths. The shear method in Figure 6.5c, combines the two discussed methods. This method becomes of interest when the colloid-wall interactions become of more significance. Even though the computation times become longer, the method is most similar to real shear systems.

A possible explanation for the weak gradient in the velocity profiles of Figures 6.3b and 6.3c can be the effect of the random forces in Langevin dynamics. The random forces are also affected by the presence of shear. This can be neglected at low shear rates, however, at higher shear rates, the effect of the random forces becomes more significant (Dhont, 1996). Kroupa et al. (2014) developed a 2D discrete element model (DEM), specifically designed to investigate the effect of shear on coagulation. In the model, he assumed that the shear forces dominate the thermal motion of the colloids; only the drag force induced by the fluid is taken into account. Therefore, the interactions between the colloidal particles and the solvent are described with Stokes law to impose a simple shear flow.

$$F_{f,\text{Kroupa}} = 6\pi\mu a(v_f - v). \tag{6.4}$$

The friction force imposed by Kroupa is of a higher magnitude than the friction force in the Langevin dynamics. High friction solvents experience more effects of the imposed shear. In Figure 6.3d the additional force is set to be $v_f - v$. In a concise time the desired velocity profile is achieved. When choosing the external force, it is important to keep the Peclet number in mind. In case the $\text{Pe} \gg 1$, it is valid to only take the friction of the fluid into account and neglect diffusion. However, for $\text{Pe} \sim 1$, having an additional force complementary to the Langevin friction force is more accurate; diffusion still has a significant contribution.

Figure 6.4 shows the radial distribution function for different imposed shear forces. The function fluctuates for both additional forces around one, the same as when no external force is added. The simulations are performed with the `MHS` pair style. The effect of shear is particularly interesting for attractive particle interactions with a repulsive barrier. Different from hard sphere interactions, the higher collision force and frequency induced by shear can trap attractive particles in a lower energy level, which can cause cluster forming. Hence, the radial distribution functions of Figure 6.4 can be explained by the hard sphere interactions between the particles. Unfortunately, due to time constraints, no further analysis is done on the obtained simulation data. The data can provide more insight into the effect of shear forces by counting the number of collisions in the simulation. This number is expected to go up with a higher velocity gradient.

The forces that are induced on the particles, currently cause a simple shear flow. Other laminar velocities profiles can be generated by adjusting the formula that describes the fluid velocity, Equation 6.3. However, at higher velocities, often turbulent flows appear. A turbulent flow contains vortexes, which are not constant over the flow direction. An approximation of the turbulent flow could be created by adding another external force in the y-direction, z-direction, or both. This force can have a sinusoidal shape, and thereby inducing an alternating up and down force on the particles. However, adding too many forces limits the freedom of the particles and thereby can reduce the fidelity of the particle behavior. Soos et al. (2008) showed that the collision efficiency (α) decreases at higher shear rates for turbulent flows, $\alpha \propto G^{-0.18}$. On the other hand, Krutzer (1993) found that the number of particle collisions was the same for both Laminar and isotropic turbulent flow. However, due to a lower stability ratio in turbulent flows, the coagulation rate was higher in an isotropic turbulent flow.

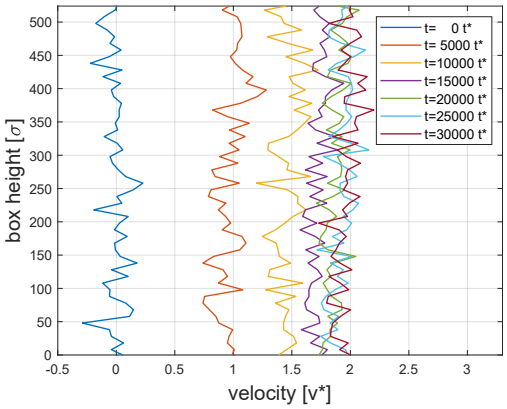

(a) Simulation box with only periodic boundaries. $F_{\text{add}} = \frac{m}{\gamma} v_f$.

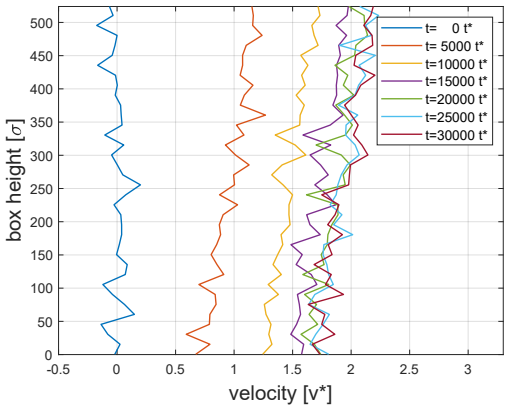

(b) Simulation box with ideal reflecting walls in the y-dimension. $F_{\text{add}} = \frac{m}{\gamma} v_f$.

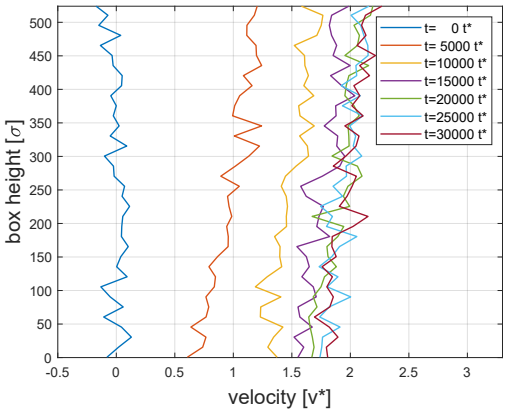

(c) Simulation box with an ideal reflecting wall at the upper edge and a 9,3-Lennard-Jones wall at the lower edge of the y-dimension. $F_{\text{add}} = \frac{m}{\gamma} v_f$.

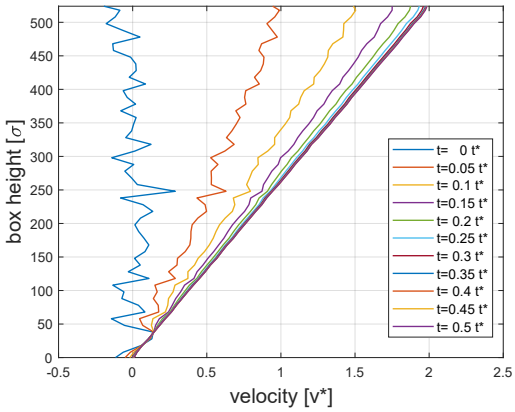

(d) Simulation box with an ideal reflecting wall at the upper edge and a 9,3-Lennard-Jones wall at the lower edge of the y-dimension. $F_{\text{add}} = v_f - v$.

Figure 6.3: The velocity profile for different simulation conditions.

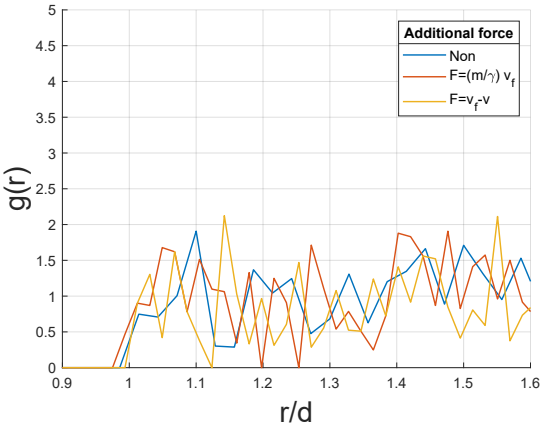

Figure 6.4: The radial distribution function for simulations with an additional force on the particles to induce a simple shear profile.

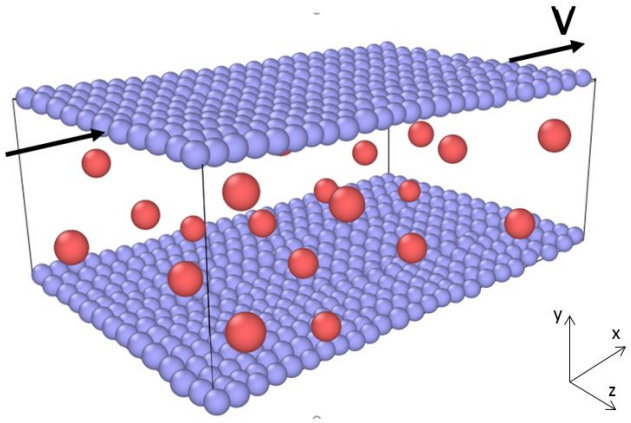

(a) A simulation box containing rough walls. The upper wall is moving.

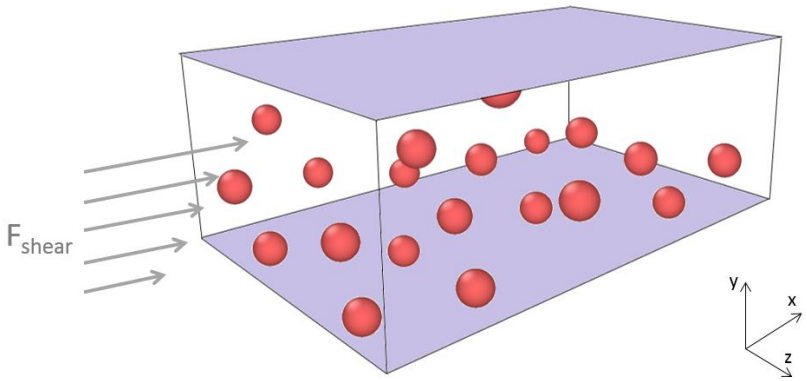

(b) A simulation box containing ideal walls.

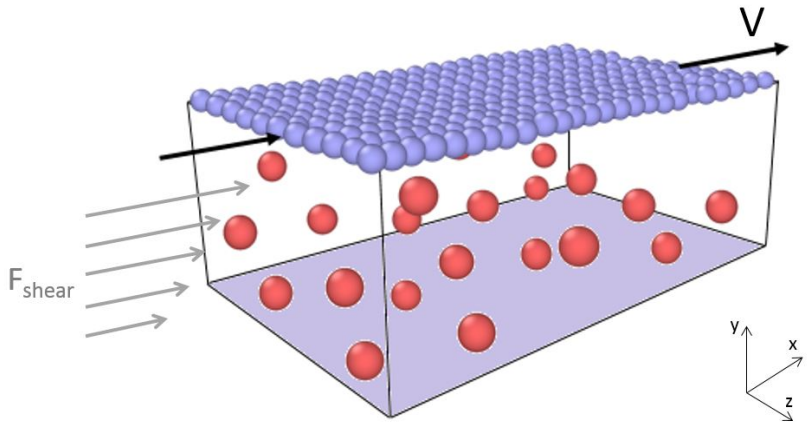

(c) A simulation box containing a rough moving wall at the top and a ideal wall at the bottom.

Figure 6.5: The different wall options to impose shear.

Chapter 7

Discussion

The new model is developed, making use of the LAMMPS code. This choice is made to save time in writing a whole new code. The code of LAMMPS is known for its computational efficiency and broad applicability. However, an already existing code confines the modeling options. Especially in the implementation of a stochastic depletion force, this is experienced as a limitation. Moreover, using an already existing program requires much exploratory work on the possibilities of the program. For that reason, a significant part of the work consists of simply understanding the technicalities of LAMMPS. This does not result in new findings, but is essential in the development of a feasible model.

Colloidal particles show Brownian behavior in the diluted regime. For this reason, the simulations are performed for low volume fractions ranging from 1 vol.% to 7 vol.%. However, polymerization systems often contain a high solid content (40vol.%∼60vol.%). The recent trend is even to increase the solid content towards 75 vol.% to improve economic productivity (Cheng et al., 2018). More importantly, systems that undergo coagulation have many local regions with a high volume fraction. The potentials that are described in this work are pair-wise potentials, which corresponds to the assumption that only binary collisions take place (Zaccone et al., 2010). For higher volume fraction, this assumption becomes less valid. Furthermore, the Langevin dynamics are less fitted to describe the fluid dynamics at high colloidal volume densities. The hydrodynamic forces become more significant, as is already elaborately discussed in section 4.1. However, at very high volume fractions and long interaction ranges, the hydrodynamic forces again can be neglected (Padding and Louis, 2006), which can be the case in the final stages of coagulation. The modeling methods discussed in chapters 5 and 6 are not worth less because of the used Langevin solvent dynamics. Other implicit solvent modeling methods experience the same obstacles in modeling polydispersity and shear effects.

This work focuses on depletion and shear forces as the leading causes of coagulation. However, as already mentioned in the theoretical background, many forces play a role in colloidal dispersions. For instance, electrostatic, steric, and solvation forces play a role in the stability of the system. It is important to have insight into the significance of these forces because the particles inducing these forces affect the quality of the final product. The addition of charged particles to a colloidal dispersion can also contribute to the destabilization of the system. The addition of salt can weaken the particle-particle repulsive electrostatic forces. The salt concentration where coagulation starts to occur is the critical coagulation concentration (ccc). In the end, the effective interaction potential is the most important gauge to predict if the system is sensible to coagulation. Shear forces can give an extra push towards lower energy states, but will not induce coagulation if no a part of the potential is negative.

Chapter 8

Conclusions

The first steps are made towards a time-driven model that can simulate colloidal behavior in non-equilibrium situations. The model is geared towards emulsion polymerization systems, but can easily be extended to every colloidal dispersion.

The open-source code of LAMMPS is used as an interface for the model, to make use of the efficient parallel programming of the program. It is found that a minimum of 1000 particles is required to obtain accurate statistics. The effect of the cutoff range is explained by an analysis on the Lennard-Jones potential. A cut-off of 150 σ is necessary to describe the potential accurately. The program capabilities are fully explored by the implementation of a new pair style for hard spheres in the code. The pair style can be used to resemble the hard sphere behavior of particles while maintaining a minimum energy error.

Furthermore, the effect of solvent dynamics is extensively investigated. The number of solvent particles relative to the number of colloids is too high to model all solvent particles explicitly. Therefore, Langevin dynamics are used to resemble the solvent effect with stochastic forces. A damping constant of 7500 is required to resemble the typical Brownian behavior of hard sphere colloidal particles in the diluted regime. For interactions beyond the hard sphere, the behavior of the particles start to deviate slightly more from theory. This is probably due to the lack of hydrodynamic forces in Langevin dynamics. At higher (local) volume fractions, hydrodynamics are required to simulate the colloidal behavior accurately. The overall trend for the Yukawa interactions is as expected; attractive interactions have the lowest diffusion coefficient and hard sphere interactions the highest.

With the tuned solvent dynamics, it is explored how to model forces that are induced by phenomena of different length scales. Polydispersity and shear are possible causes of coagulation phenomena in colloidal dispersions. Small particles in the dispersion can induce depletion forces. At least 22 million depletant particles are required to model an interaction strength of $-5k_BT$. Modeling these particles explicitly, is not feasible. Therefore, the depletion potential for hard sphere depletants is reproduced with a sum of multiple Yukawa potentials. Two fitting methods are discussed, of which the minimization method allowed for the best fit. Five Yukawa tails are required.

Moreover, shear is a macroscopic phenomenon, which has its effect on the mesoscopic colloidal particles. It induces a fluid flow, which increases the frequency and speed of the collisions. Several methods are discussed to obtain a simple shear flow. Rough moving walls are most realistic, however, are computationally very expensive. The addition of an external force to increase the experienced friction force creates a simple shear flow. The gradient of the shear flow increases as the friction force increases. The colloid-wall interactions do not affect the velocity profile of the particles.

Summarizing, the model is capable of accurately predicting colloidal dynamics in the diluted regime. Several methods have been suggested to model coagulation effects induced by phenomena of differ-

ent length scales. However, the model needs further development to model coagulation effects with high fidelity.

Chapter 9

Outlook

This work being a first step in the development of a model allows for an elaborate outlook. The model is developed to obtain more insight in coagulation phenomena of colloidal dispersions. To investigate the effect of certain parameters on the behavior of the colloidal particles, the fidelity of the physical properties is essential.

A considerable improvement can be made in the solvent dynamics. The dynamics are currently modeled by a Langevin thermostat. However, this thermostat does not have the hydrodynamic forces incorporated. These forces become more critical as the colloidal density of the dispersion increases. Wang (Wang et al., 2016) introduced a software package for fluctuation hydrodynamics simulations of fluid-structure interactions subject to thermal fluctuations. This software is integrated with LAMMPS. A stochastic Eulerian Lagrangian method SELM is used to couple coarse-grained microstructure degrees of freedom to continuum stochastic fields. It would be interesting to compare the SELM and Langevin solvent dynamics for both low and high density systems.

The depletion potential that is used to describe the effect of polydispersity in this work is specified for hard sphere colloids and hard sphere depletants. In colloidal dispersions, often free polymers are dissolved in the bulk phase. These polymers can also induce a depletion interaction between the colloidal particles. The depletion potential induced by free polymers can be described by the potential for hard sphere colloids and penetrable hard spheres (Lekkerkerker and Tuinier, 2011). The two depletion potentials can be compared to investigate which depletant particles have the highest contribution to the clustering of the particles. Moreover, the depletion potential is currently represented by an n-tails Yukawa potential. However, it is also possible to implement a new pair style in LAMMPS that induces the depletion potential on the colloidal particles. This can be done with the `colloid` pair style as a reference pair style. The depletion potential would require three input arguments; the colloid size, the depletant size, and the depletant volume fraction. Pair style `colloid` has sufficient arguments for this.

Regarding the implementation of shear at implicit solvent systems, the addition of an external force has a significant effect. However, the colloid-wall interactions do not contribute to the simple shear velocity profile. With a more advanced implicit solvent method, the effect of the volume density on the significance of colloid-wall interactions can be investigated. Furthermore, the attraction strength of the walls can be increased to enhance the energy favor that the particles experience near the wall. The currently used ideal walls, *reflect* and *lj93*, are both smooth walls. One of the implemented ideal walls in LAMMPS, *fix wall/gran*, creates frictional walls. This wall can be used for the lower edge to slow down the particles.

Validation of the model is required to test the accuracy of the simulations. The behavior of the colloidal particles can be studied experimentally by techniques such as light scattering and optical microscopy. The properties of colloidal can be tuned by, for instance, grafting the surface of the particles with poly-

mers (Dullens, 2005). These tailor-made particles allow for extensive validation. The hard sphere simulations, which have been predominantly discussed in this work, can be experimentally be validated with sterically stabilized polymethyl methacrylate (PMMA) colloids or silica spheres (Dullens, 2005).

In a later stage of the model development, more advanced improvements can be made. It would be interesting to investigate the effect of different flow types. It may well be that turbulent flow causes less coagulation than laminar flow, due to the higher velocities. Moreover, the particle shape and deformation can play an important role in cluster formation. The particle potentials vary for different geometries (Cheng et al., 2018). Lastly, multiple phenomena can be combined. The depletion forces can be induced at the same time as the shear forces. However, the depletion forces alter in the presence of shear (July et al., 2012), this has to be taken into account.

Chapter 10

Acknowledgment

Firstly, I would like to thank Remco Tuinier and Ivo Roghair for providing me the opportunity to perform this project. I always enjoyed our two-weekly meetings. It was very inspiring for me to see your enthusiasm for the project, especially for new topics not within your own expertise area. Besides the two-weekly meetings, you always made room for me in your schedule if I had a question, I appreciate this very much, knowing how busy you are.

In addition, the return of Mark Vis from Lyon has been very valuable for me. Since he came back, he has been a great help in the proceeding of my project. He even became a permanent member of the meetings with Remco and Ivo. I have enjoyed our discussion on data interpretation and learned a lot from your experience with LAMMPS.

Furthermore, I have always felt very welcome in the SPC group. In the group is a right balance between fun and work, which is a nice environment to work in. The critical questions asked in theory group meetings and Friday afternoon meetings have always been very much appreciated. Especially, I would like to thank SPC members Álvaro González García and Mark Vis, who helped to develop the Mathematica scripts that has been used to fit the n-tails Yukawa potential. Another valued (ex)-SPC member is my colleague from the 'Bollenbak', Max Schelling. We have always had a pleasant atmosphere in our office, it was unfortunate that it ended so abruptly with introduction of COVID-19.

Lastly, I would like to thank my family and friends. The daily tea-breaks with Nikolaj, Luuk, and Thomas were the moments that I could charge up for the rest of the day and I am happy that we proceeded the breaks even in an online setting. Edith, Stefan, Lotte, and Lennard are closest to me. They always gave me confidence by telling me that they are proud of me, no matter what the final result is.

List of Symbols

Abbreviations

HS	Hard sphere
LJ	Lennard-Jones
MHS	Mie hard sphere
MSD	Mean square displacement
RAM	Random access memory

Greek symbols

α	Collision efficiency	
δ	Width of the attractive well	m
ϵ	Minimum energy of a LJ potential	J
γ	Damping constant	s
κ^{-1}	Screening length	m
μ	Fluid viscosity	$\mathrm{kg\,m^{-1}\,s^{-1}}$
ϕ	Colloid volume fraction	
σ	Diameter solvent particle	m
τ	Stickiness parameter	

Latin symbols

A	Hamaker constant	J
a	Particle radius	m
B_2	Second virial coefficient	$\mathrm{m^3\,mol^{-1}}$
d	Particle diameter	m
D_0	Ideal diffusion coefficient	$\mathrm{m^2\,s^{-1}}$
D_s	Self-diffusion coefficient	$\mathrm{m^2\,s^{-1}}$
F	Force	N
h	Interparticle surface distance	m
k_B	Boltzmann constant	$\mathrm{m^2\,kg\,s^{-2}\,K^{-1}}$

m	Particle mass	kg
N	Number of particles	
p	Position coordinate	
r	Interparticle centre distance	m
T	Temperature	K
t	Time	s
U	Potential energy	J
V	Wall velocity	$\mathrm{m\,s^{-1}}$
v	Particle velocity	$\mathrm{m\,s^{-1}}$
v_c	Volume of a colloid	$\mathrm{m^3}$
v_f	Fluid velocity	$\mathrm{m\,s^{-1}}$

Bibliography

J. M. Asua. Challenges and Opportunities in Continuous Production of Emulsion Polymers: a Review. *Macromolecular Reaction Engineering*, 10(4):311–323, 2016. ISSN 18628338. doi: 10.1002/mren.201500032. 4

G. K. Batchelor. Brownian diffusion of particles with hydrodynamic interaction. *Journal of Fluid Mechanics*, 74(1):1–29, 1976. ISSN 14697645. doi: 10.1017/S0022112076001663. 6

R.J. Baxter. Percus – Yevick Equation for Hard Spheres with Surface Adhesion. *Journal of Chemical Physics*, 49, 1968. doi: https://doi.org/10.1063/1.1670482. 7, 26

D. Cheng, S. Ariafar, N. Sheibat-Othman, J. Pohn, and T.F.L. McKenna. Particle Coagulation of Emulsion Polymers: A Review of Experimental and Modelling Studies. *Polymer Reviews*, 58(4):717–759, 2018. ISSN 15583716. doi: 10.1080/15583724.2017.1405979. 1, 3, 4, 35, 41, 46

B. Cichocki and B. U. Felderhof. Diffusion coefficients and effective viscosity of suspensions of sticky hard spheres with hydrodynamic interactions. *The Journal of Chemical Physics*, 93(6):4427–4432, 1990. ISSN 00219606. doi: 10.1063/1.459688. 7

B. Cichocki, M. L. Ekiel-Jeżewska, and E. Wajnryb. Lubrication corrections for three-particle contribution to short-time self-diffusion coefficients in colloidal dispersions. *The Journal of Chemical Physics*, 111(7):3265–3273, 1999. ISSN 0021-9606. doi: 10.1063/1.479605. 6

J.K.G. Dhont. *An introduction to Dynamics of colloids*. Elsevier Science B.V., Amsterdam, first edition, 1996. ISBN 0444820094. 2, 4, 5, 6, 25, 35, 37, 38

M. Dijkstra, R. Van Roij, R. Roth, and A. Fortini. Effect of many-body interactions on the bulk and interfacial phase behavior of a model colloid-polymer mixture. *Physical Review E - Statistical, Nonlinear, and Soft Matter Physics*, 73(4):1–14, 2006. ISSN 15393755. doi: 10.1103/PhysRevE.73.041404. 29

D. Distler. Emulsion polymerization. In *Encyclopedia of Materials: Science and Technology*, pages 2769–2774. Elsevier, 2nd edition, 2001. ISBN 0-08-0431526. doi: 10.1016/B0-08-043152-6/00493-9. 3

D. Distler, W.S. Neto, and F. Machado. Emulsion polymerization. In *Reference Module in Materials Science and Materials Engineering*, pages 35–56. Elsevier, 2017. doi: 10.1016/B978-0-12-803581-8.03746-2. 1, 3

R. Dullens. *Structure and dynamics of colloidal hard spheres in real-space*. PhD thesis, Utrecht university, 2005. 6, 46

A.N.M.W. El-hoshoudy. Emulsion polymerization mechanism. *IntechOpen*, 2018. doi: 10.5772/intechopen.72143. 4

R. C. Elgebrandt, J. A. Romagnoli, D. F. Fletcher, V. G. Gomes, and R. G. Gilbert. Analysis of shear-induced coagulation in an emulsion polymerisation reactor using Computational Fluid Dynamics. *Chemical Engineering Science*, 60:2005–2015, 2005. doi: 10.1016/j.ces.2004.12.010. 1

R. Everaers and M. R. Ejtehadi. Interaction potentials for soft and hard ellipsoids. *Physical Review E*, 67(4), 2003. ISSN 1063651X. doi: 10.1103/PhysRevE.67.041710. 17

A. Fortini, M. Dijkstra, and R. Tuinier. Phase behaviour of charged colloidal spheredispersions with added polymer chains. *journal of physics: condensed matter*, 17:7783–7803, 2005. doi: 10.1088/0953-8984/17/50/002. 2, 15

D. Frenkel and Berend Smit. *Understanding molecular simulation; From Algorithms to Applications*. Academic Press, San Diego, San Francisco, New york, Boston, London, Sydney, Tokyo, 2nd edition, 1996. ISBN 0-12-267351-4. 12, 19, 21

G. Gallavotti. *Statistical mechanics; a short treatise*. Springer, Heidelberg, 1999. ISBN 9783642624759. doi: 10.1007/978-3-642-56680-6. 19

G. Gompper, T. Ihle, D.M. Kroll, and R.G. Winkler. Multi-Particle Collision Dynamics: A Particle-Based Mesoscale Simulation Approach to the Hydrodynamics of Complex Fluids. In *Advanced Computer Simulation Approaches for Soft Matter Sciences III*, chapter 1, pages 1–87. Springer, 2009. 22

I. González, M. Paulis, J.C. de la Cal, and J. Asua. (Mini)emulsion Polymerization: Effect of the Segregation Degree on Polymer Architecture. *Macromolecular Reaction Engineering*, 1(6):635–642, 2007. ISSN 1862832X. doi: 10.1002/mren.200700031. 1

Á. González García. *Polymer-mediated phase stability of colloids*. PhD thesis, Eindhoven University of Technology, 2019. 31

Á. González García and R. Tuinier. Tuning the phase diagram of colloid-polymer mixtures via Yukawa interactions. *Physical Review E*, 94(6), 2016. ISSN 24700053. doi: 10.1103/PhysRevE.94.062607. 15, 29

G. S. Grest and K. Kremer. Molecular dynamics simulation for polymers in the presence of a heat bath. *Physical Review A*, 33(5):3628–3631, 1986. ISSN 10502947. doi: 10.1103/PhysRevA.33.3628. 19

H. F. Hernandez and K. Tauer. Brownian dynamics and kinetic Monte Carlo simulation in emulsion polymerization. *Computer Aided Chemical Engineering*, 25:769–774, 2008. ISSN 15707946. doi: 10.1016/S1570-7946(08)80134-4. 4

S. Iqbal and S. Ahmad. Recent development in hybrid conducting polymers: Synthesis, applications and future prospects. *Journal of Industrial and Engineering Chemistry*, 60:53–84, 2018. ISSN 22345957. doi: 10.1016/j.jiec.2017.09.038. 3

J. Jover, A. J. Haslam, A. Galindo, G. Jackson, and E. A. Müller. Pseudo hard-sphere potential for use in continuous molecular-dynamics. *Journal of Chemical Physics*, 137(14), 2012. ISSN 00219606. doi: 10.1063/1.4754275. 15

C. July, D. Kleshchanok, and P. R. Lang. Shear-affected depletion interaction. *European Physical Journal E*, 35(7), 2012. ISSN 12928941. doi: 10.1140/epje/i2012-12060-7. 46

M. Kroupa, M. Vonka, and J. Kosek. Modeling the Mechanism of Coagulum Formation in Dispersions. *Langmuir*, 30(10):2693–2702, mar 2014. ISSN 0743-7463. doi: 10.1021/la500101x. 1, 38

L.L.M. Krutzer. *The influence of flow type, particle type and gravity on orthokinetic coagulation*. PhD thesis, Eindhoven University of Technology, 1993. 38

R. Kubo. The fluctuation-dissipation theorem. *Reports on Progress in Physics*, 29, 1966. 22

M. Lattuada and M. Morbidelli. Effect of Repulsive Interactions on the Rate of Doublet Formation of Colloidal Nanoparticles in the Presence of Convective Transport. *journal of colloid interface science*, 355(1):42–53, 2011. doi: 10.1016/j.jcis.2010.11.070. 1

M. Laurati, G. Petekidis, N. Koumakis, F. Cardinaux, A. B. Schofield, J. M. Brader, M. Fuchs, and S. U. Egelhaaf. Structure, dynamics, and rheology of colloid-polymer mixtures: From liquids to gels. *Journal of Chemical Physics*, 130(13), 2009. ISSN 00219606. doi: 10.1063/1.3103889. 4

A. R. Leach. *Molecular Modelling: Principles and Applications*. Pearson Education Limited, 2001. ISBN 9780582382107. 13

H. N. W. Lekkerkerker and R. Tuinier. *Colloids and the Depletion interaction*. Springer Berlin Heidelberg, 2011. ISBN 978-94-007-1222-5. doi: 10.1007/978-94-007-1223-2. 4, 29, 45

R. Lewarchik. The Fundamentals of Emulsion Polymerization, 2016. URL `https://knowledge.ulprospector.com/4911/pc-fundamentals-emulsion-polymerization/`. 3

A. Malevanets. Mesoscopic model for solvent dynamics. *Journal of Chemical Physics*, 110(17):8605–8613, 1999. ISSN 00219606. doi: 10.1063/1.478857. 21

M.J.J Mayer. *The dynamics of batch and continuous emulsion polymerization*. PhD thesis, Eindhoven university of technology, 1995. 1

H. Namazi. Polymers in our daily life. *Bioimpacts*, 7(2):73–74, 2017. doi: 10.15171/bi.2017.09. 1

M.G. Noro and D. Frenkel. Extended corresponding-states behavior for particles with variable range attractions. *Journal of Chemical Physics*, 113(8), 2000. doi: https://doi.org/10.1063/1.1288684. 31

K. Ouzineb, C. Graillat, and T. McKenna. Continuous tubular reactors for latex production: Conventional emulsion and miniemulsion polymerizations. *Journal of Applied Polymer Science*, 91(4):2195–2207, 2004. ISSN 00218995. doi: 10.1002/app.13340. 4

J. T. Padding and A. A. Louis. Hydrodynamic interactions and Brownian forces in colloidal suspensions: Coarse-graining over time and length scales. *Physical Review E - Statistical, Nonlinear, and Soft Matter Physics*, 74(3):1–29, 2006. ISSN 15393755. doi: 10.1103/PhysRevE.74.031402. 22, 41

W. Pauer. Reactor concepts for continuous emulsion polymerization. In *Polymer reactor engineering for dispersed systems*, chapter 1. Springer, 1 edition, 2017. ISBN 978-3-319-73479-8. doi: https://doi.org/10.1007/978-3-319-73479-8. 1

B. Pinter, T. Fievez, F. M. Bickelhaupt, P. Geerlings, and F. de Proft. On the origin of the steric effect. *Physical Chemistry Chemical Physics*, 14(28):9846–9854, 2012. ISSN 14639076. doi: 10.1039/c2cp41090g. 4

S. Plimpton. Re:[lammps-users] Hard sphere potential, 2009. URL `https://lammps.sandia.gov/threads/msg08499.html`. 15

S. Plimpton. LAMMPS Features and Capabilities, 2014. URL `https://lammps.sandia.gov/tutorials/italy14/italy{_}overview{_}Mar14.pdf`. 2, 9, 10

S. Plimpton, A. Thompson, S. Moore, A. Kohlmeyer, and R. Berger. LAMMPS, 2020. 9, 16

R. Pokorný, A. Zubov, P. Matuška, F. Lueth, W. Pauer, H. U. Moritz, and J. Kosek. Process Model for Styrene and n-Butyl Acrylate Emulsion Copolymerization in Smart-Scale Tubular Reactor. *Industrial and Engineering Chemistry Research*, 55(2):472–484, 2016. ISSN 15205045. doi: 10.1021/acs.iecr.5b02909. 4

W.C.K. Poon. Colloids as big atoms: The genesis of a paradigm. *Journal of Physics A: Mathematical and Theoretical*, 49(40):1–3, 2016. ISSN 17518121. doi: 10.1088/1751-8113/49/40/401001. 4

C. Regnaut and J. C. Ravey. Application of the adhesive sphere model to the structure of colloidal suspensions. *The Journal of Chemical Physics*, 91(2):1211–1221, 1989. ISSN 00219606. doi: 10.1063/1.457194. 26

V. Rühle. Berendsen and Nose-Hoover thermostats. Technical report, 2007. 19

W.B. Russel, D.A. Saville, and W.R. Schowalter. *Colloidal Dispersions*. Cambridge University Press, 1991. ISBN 0521426006. 5

Sandia Corporation. LAMMPS documentation, 2020. URL `https://lammps.sandia.gov/doc/Manual.html`. 9, 10, 11, 19, 22, 26, 37, 59

T. Schlick. *Molecular Modelling and Simulation: An interdisciplinairy guide*, volume 21. Springer, second edition, 2010. ISBN 9780387877075. doi: 10.1007/978-0-387-75847-3. 22

Y. Shen, D. Xiang, X. Wang, L. Jiang, and Y. Wei. A contact force model considering constant external forces for impact analysis in multibody dynamics. *Multibody System Dynamics*, 44(4):397–419, 2018. ISSN 1573272X. doi: 10.1007/s11044-018-09638-0. 11

M. Soos, A.S. Moussa, L. Ehrl, J. Sefcik, H. Wu, and M. Morbidelli. Effect of shear rate on aggregate size and morphology investigated under turbulent conditions in stirred tank. *Journal of Colloid and Interface Science*, 319(2):577–589, 2008. ISSN 00219797. doi: 10.1016/j.jcis.2007.12.005. 38

M. Tuckerman, B. J. Berne, and G. J. Martyna. Reversible multiple time scale molecular dynamics. *The Journal of Chemical Physics*, 97(3):1990–2001, 1992. ISSN 00219606. doi: 10.1063/1.463137. 12

Y. Wang, J.K. Sigurdsson, and P.J. Atzberger. Fluctuating hydrodynamics methods for dynamic coursgrained implicit-solvent simulations in LAMMPS. *SIAM Journal on Scientific Computing*, 38(5):62–77, 2016. doi: 10.1137/15M1026390. 22, 23, 45

Wolfram. Numerical Nonlinear Global Optimization, 2020. URL `https://reference.wolfram.com/language/tutorial/ConstrainedOptimizationGlobalNumerical.html`. 62

H.B. Yamak. Emulsion Polymerization: Effects of Polymerization Variables on the Properties of Vinyl Acetate Based Emulsion Polymers. *Polymer science*, 2013. doi: 10.5772/51498. 3, 4

A. Zaccone, D. Gentili, H. Wu, and M. Morbidelli. Shear-induced reaction-limited aggregation kinetics of Brownian particles at arbitrary concentrations. *Journal of Chemical Physics*, 132(13), 2010. ISSN 00219606. doi: 10.1063/1.3361665. 41

A. Z. Zinchenko and R. H. Davis. Collision rates of spherical drops or Particles in a shear flow at arbitrary Peclet numbers. *physics of fluids*, 7:2310–2327, 1995. doi: doi:10.1063/1.868745. 1

Appendix A

Example input script

In this appendix one of the input scripts is given as an example. This input script is used to perform a simulation for hard sphere colloidal particles of size 14σ with implicit solvent dynamics.

```
# Sets respectively the units, the quantities coupled to the particles,
# and the number of dimension of the simulation.
units           lj
atom_style      sphere
dimension       3

# Creates the simulation box and indicates the number of particle
# types in the system.
region          box block 0 524 0 524 0 524
create_box      1 box

# Input of colloidal particles
read_data       c_inp.000.d14 add append

# Set the initial velocity
velocity        all create 1.0 3344508

# Sets the properties of the colloids and puts all particles of type 1
# in one group.
set             type 1 mass 9
set             type 1 diameter 14
group           colloid type 1

# Determines how and when the neigbourlist is built and how it is
# communicated between the processors.
neighbor        1 multi
neigh_modify    delay 0
neigh_modify    one 10000
comm_modify     mode multi

###----------------- Potentials and time integration ---------------
# Set the pair interaction
pair style      MHS 15
pair_coeff      1 1 1.0 1.0 14.0 14.0

# Set the time integration, by choosing the ensemble and thermostat
```

```
fix             1 all nve
fix             2 all langevin 1.0 1.0 7500.0 9234987

###----------------------------- Output -----------------------------
dump            1 all atom 1000 dump.OvitoT1D14
dump            dmp2 colloid custom 1000 dump*.Matlab id x y z vx vy vz
dump            dmp2 pad 9
thermo_style    custom step time etotal epair e kin press vol
thermo          1000

###------------------------------ run -------------------------------
timestep        0.001
run             30000000
```

Appendix B

Lennard-Jones units

In the Lennard-Jones units, all quantities are unitless. There are three fundamental quantities; σ, ϵ, and m. These quantities are set to 1. All other quantities are multiples of those three. By chosing specific values for σ, ϵ, and m, all units can be converted to real units. The LJ units as they are defined in LAMMPS are shown below (Sandia Corporation, 2020).

Quantity	Real unit	LJ unit	Simplified LJ unit
Mass	kg	m	
Distance	m	σ	
Energy	J	ϵ	
Time	s	$\sqrt{m\sigma^2/\epsilon}$	t^*
Velocity	m/s	$\sqrt{\epsilon/m}$	v^*
Force	N	ϵ/σ	f^*
Temperature	K	ϵ/k_B	T^*
Pressure	Pa·s	ϵ/σ^3	p^*
Dynamic viscosity	μ	$\epsilon\tau/\sigma^3$	μ^*
Density	ρ	m/σ^{-3}	ρ^*
Diffusion coefficient	m^2/s	$\sqrt{\sigma^2\epsilon/m}$	D^*

Appendix C

Box Length for a square simulation box

In this appendix the box lengths are listed for a cubic simulation box. Furthermore, the mass density as function of the volume fraction is given.

	Number of particles		
Colloid diameter [σ]	12	100	1000
14	76	153	330
16	86	175	330
18	97	197	424
20	108	219	471

Table C.1: The box length in σ for a cubic box. The density is kept constant at 4 %vol. The number of particles is varied.

	Volume fraction colloids						
Colloid diameter [σ]	1 %	2 %	3%	4%	5%	6%	7%
14	524	416	363	330	306	288	274
16	599	475	415	377	350	329	313
18	673	534	467	424	394	371	391
20	748	594	519	471	438	412	391

Table C.2: The box length in σ for a cubic box. The box contains 1000 particles and the volume density of those particles is varied.

Volume fraction colloids	1%	2%	3%	4%	5%	6%	7%
Mass density	6.26e-5	1.24e-4	1.88e-4	2.51e-4	3.13e-4	3.76e-4	4.38e-4

Table C.3: The colloidal mass density of the system as a function of the colloid volume fraction.

Appendix D

The radial distribution function of the attractive hard sphere Yukawa potential

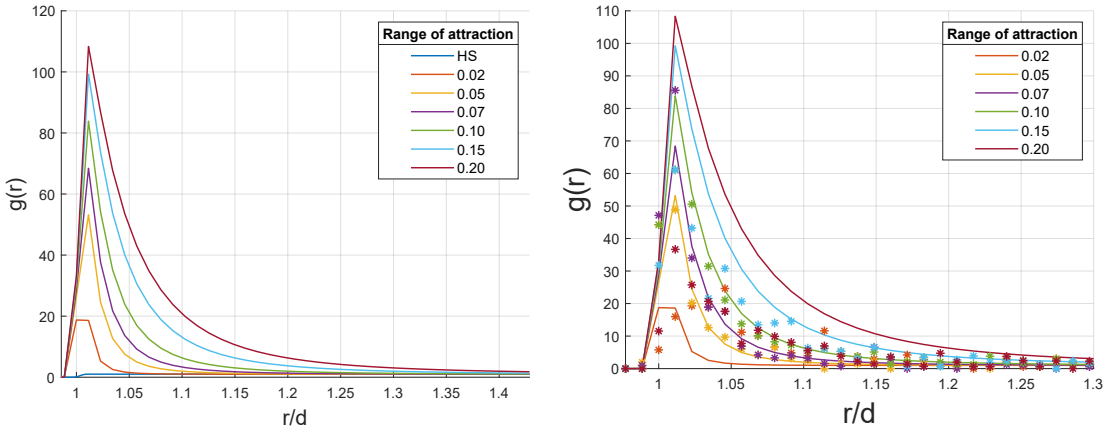

(a) The binned version of the theoretical radial distribution function.

(b) The theoretical radial distribution function (lines) compared to the simulation radial distribution function (stars).

Figure D.1: The binned radial distribution functions depending on the range of attraction. Binsize=0.011.

Appendix E

Minimization methods for the Yukawa fitting

The Yukawa fitting is performed with four different minimization tools. These tools are all incorporated in Mathematica (Wolfram, 2020). In this appendix these tools are shortly explained. Futhermore, in the tables the computation times and minimized errors are listed for the different tools. These fittings are performed to recreate the depletion potential for a colloid-to-depletant ratio of 100.

RandomSearch
This algorithm generates a population of random starting points and performs a local optimization from each starting point to converge to a minimum.

DifferentialEvolution
This algorithm is a simple stochastic function minimizer. During each iteration a population of points is generated. The new points are compared to the points of the old iteration. If the function value is lower with the new point value, the old one is replaced. In case the function values in the old and new populations, as well as the distance between the new best point and the old best point are below a set tolerance, the process is converged.

SimulatedAnnealing
Like RandomSearch, this algorithm uses multiple starting points. Every iteration a new point is generated. This point is in the neighborhood of the previous point. If the new point is lower than the current best point, the best point is replaced. In case it is not smaller the old point is replaced with a probability e^b. In which b is the boltzmann exponent.

NelderMead
This algorithm is a direct search method. For a function with n variables, a set of $n+1$ points forming vertices of a polytope is created. The points are ordered based on magnitude of the function value. The point with the highest function value is replaced. This continues in the further iterations. When the best function values in the new and old polytope and the distance between the new and best point are below the tolerance, the process is converged.

	Fitting method	**RandomSearch**	**DifferentialEvolution**	**SimulatedAnnealing**	**NelderMead**
2 tails	standard deviation	0.055	0.094	0.094	0.032
	computation time	0:39	0:05	0:04	0:07
3 tails	standard deviation	0.032	0.067	0.094	0.032
	computation time	3:20	0:13	0:06	0:07
4 tails	standard deviation	0.020	0.067	0.094	0.055
	computation time	10:41	0:18	0:08	0:15
5 tails	standard deviation	0.016	0.027	0.067	0.494
	computation time	27:54	0:40	0:16	0:12
6 tails	standard deviation	0.014	0.067	0.032	0.170
	computation time	55:17	0:33	0:36	0:12

Table E.1: The minimized error and computation time for four minimization methods. The fitting is performed on a depletion potential with q=0.01.

Appendix F

Fitted Yukawa parameters

	tail 1		tail 2		tail 3		tail 4		tail 5	
depletant-to-colloid ratio (q)	A	κ	A	κ	A	κ	A	κ	A	κ
0.1	1145.03	21.07	-4337.26	30.13	-143.68	15.18	-1731.21	53,80	4955.80	39.27
0.02	967.11	21.75	-950.08	13.35	497.55	9.48	-120.97	7.54	-444.89	31.54
0.01	-223.78	7.55	504.17	5.65	-528.02	3.79	-62.37	2.34	295.22	2.91

Table F.1: The Yukawa parameters fitted to the depletion potential for a 5 summed Yukawa potentials.

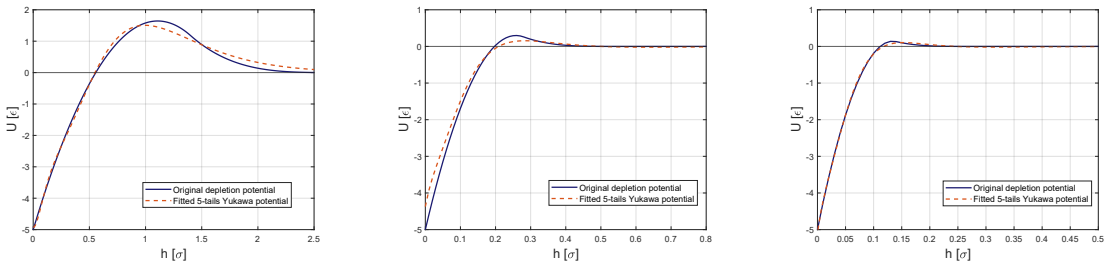

(a) q=0.1. (b) q=0.02. (c) q=0.01.

Figure F.1: The fitted 5-tails Yukawa potentials with the corresponding depletion potential.